Anal Bioanal Chem (2011) 399:2597–2622
DOI 10.1007/s00216-010-4063-3

REVIEW

Recent advances in SALDI-MS techniques and their chemical and bioanalytical applications

K. P. Law · James R. Larkin

Received: 16 May 2010 / Revised: 18 July 2010 / Accepted: 23 July 2010 / Published online: 21 August 2010

Abstract Although laser desorption mass spectrometry was introduced in the 1960s, the potential of laser mass spectrometry was not realised until the introduction of matrix-assisted laser desorption/ionisation (MALDI) in the 1980s. The technique relies on light-absorbing compounds called matrices that are co-crystallised with the analyte to achieve high ionisation and desorption efficiencies. MALDI offers a lot of advantages and is an indispensable tool in macromolecule analysis. However, the presence of the matrix also produces a high chemical background in the region below *m/z* 700 in the mass spectrum. Surface-assisted laser desorption/ionisation (SALDI) substitutes the chemical matrix of MALDI for an active surface, which means that matrix interference can be eliminated. SALDI mass spectrometry has evolved in recent years into a technique with great potential to provide insight into many of the challenges faced in modern research, including the growing interest in "omics" and the demands of pharmaceutical science. A great variety of materials have been reported to work in SALDI. Examples include a number of nanomaterials and surfaces. The unique properties of nanomaterials greatly facilitate analyte desorption and ionisation. This article reviews recent advances made in relation to carbon- and semiconductor-based SALDI strategies. Examples of their environmental, chemical and biomedical applications are discussed with the aim of highlighting progression in the field and the robustness of the technique, as well as to evaluate the strengths and weaknesses of individual approaches. In addition, this article describes the physical and chemical processes involved in SALDI and explains how the unique physical and electronic properties of nanostructured surfaces allow them to substitute for the matrix in energy transfer processes.

Keywords SALDI · DIOS · NALDI · Nanomaterial · Laser mass spectrometry

Published in the special issue on *Advances in Analytical Mass Spectrometry* with Guest Editor Maria Careri.

K. P. Law (✉)
Centre for Analytical Bioscience and Laboratory of Biophysics and Surface Analysis, School of Pharmacy, University of Nottingham, Nottingham NG7 2RD, UK
e-mail: kai.law@ntlworld.com

K. P. Law · J. R. Larkin
Clinical Sciences Research Institute, Warwick Medical School, University of Warwick, University Hospital, Clifford Bridge Road, Coventry CV2 2DX, UK

Introduction

Surface-assisted laser desorption/ionisation mass spectrometry (SALDI-MS) was originally proposed by Sunner and Chen as early as 1995 [1]. Graphite particles between 2–150 μm in size were used as ion emitters in a technique referred to here as graphite SALDI. Graphite was thought to be a suitable substrate because it is chemically inert, electroconducting and can serve as an energy receptacle for laser radiation. Subsequent development adopted a thin layer of activated carbon particles immobilised on an aluminium support [2]. Sunner referred to this approach as SALDI-MS in order to emphasise that surfaces and surface structures are critical not only to sample preparation but also to the desorption/ionisation process [2]. Although the original SALDI investigation was inspired by the early work of Tanaka et al., in which fine cobalt particles were used to couple the laser energy into a glycerol solution [3],

in practice the upper mass limit and the sensitivity of the two approaches differed greatly. Since then, a multitude of different surfaces have been reported to work as SALDI substrates with varying degrees of success. Based on the elemental composition, the majority of the SALDI substrates reported in the literature can be classified into three main types: carbon-based, semiconductor-based and metallic-based. However, this classification is insufficient. For example, depending on the molecular structure or atomic arrangement, pure carbon can range from being a pure insulator (diamond) to semiconducting (semiconducting nanotubes) and metallic (metallic nanotubes and graphite). While it is not a popular SALDI substrate of choice, silica sol-gel has also been reported as a SALDI substrate [4, 5]. Since the first report of the SALDI technique, a number of notations have been used by different authors. Some authors have termed the SALDI technique "matrix-free" or "matrix-less" laser desorption/ionisation (LDI), while others have referred to it as matrix-assisted laser desorption/ionisation (MALDI) using an inorganic matrix [6–8]. These terms have also been used interchangeably with desorption/ionisation on silicon (DIOS) [9, 10] when a porous silicon (PSi) surface is used, and nanowire-assisted laser desorption/ionisation (NALDI) [11, 12] when a surface of nanowires is used. IUPAC's provisional recommendation for the Standard Definitions of Terms Relating to Mass Spectrometry (2006), and subsequent revisions of this, defined "SALDI" as MALDI using a liquid plus particulate matrix [13]. Neither the definition of "DIOS" nor that of "NALDI" were included in the final submitted document. Opinion on the nomenclature of the technique remains divided. There have also been somewhat divided opinions and controversy regarding the optimisation of the method and the ionisation mechanism. The physical processes proposed in the literature were often speculations that were not supported by experimental evidence.

As discussed in a review prepared by He et al. [14], the initial development of graphite SALDI failed to capture the attention or imagination of the wider scientific community. This position changed after the introduction of nanomaterials as SALDI substrates. The technique has since been rediscovered as a potentially viable method to address the challenges of systems biology, particularly metabolomics, and other areas of analytical chemistry. This is because SALDI has the advantages of being high throughput, free of matrix interferences in the low-mass region of the mass spectrum, and capable of the global profiling of complex biological matrices and tissue imaging. The SALDI technique is defined here as a collection of technologies that exploit novel materials and advanced surface science for the application of laser mass spectrometry. To qualify as a SALDI technique, the authors also propose that a technique should have the following characteristics:

1. The LDI performance should be much higher than that of direct laser desorption. A sanded metal or silicon surface should only serve as an experimental control.
2. Laser fluence required to achieve LDI should be no more than the normal operation of MALDI using conventional organic matrices.
3. Being a soft ionisation technique, molecular ions, or quasi-molecular ions of the analyte should dominate the mass spectra.
4. If fragmentation occurs, the fragmentation pattern should be both orderly and predictable.
5. A wide range classes of compounds could be analysed by the technique.

This critical review addresses recent advances or strategies in relation to carbon-based and semiconductor-based SALDI techniques whilst weighing up the pros and cons of each technique with regards to both chemical and biomedical applications.

Carbon nanotubes and carbon-based SALDI

Carbon nanotubes (CNTs) were discovered in 1991 [15], and, like fullerenes, are macromolecules of elemental carbon. They can be thought of as a graphene sheet rolled into a cylinder. These intriguing structures have sparked much excitement in recent years, and a large amount of research has been dedicated to their understanding. CNTs are categorised as either single-walled nanotubes (SWNTs) or multi-walled nanotubes (MWNTs). Vertically aligned SWNTs reportedly exhibit optical properties that are very close to those of the ideal black body in the spectral range from UV to far infrared; even closer than those of super black (a chemically etched nickel–phosphorus alloy) [16]. This makes CNTs an ideal material to couple laser radiation for the application of laser mass spectrometry [17]. The use of CNTs as a carbon-based SALDI substrate has been the subject of several reviews [7, 18, 19]. Most noticeably, CNTs gave a far superior LDI performance than activated carbon. Chemically treated CNTs also exhibited an extended mass range to 12 kDa (cytochrome c). Several shortcomings encountered in the initial works were resolved by immobilisation and oxidation treatments. CNTs could also act as an SPE sorbent to extract drug molecules from urine, which were then analysed directly by SALDI-MS [20–25].

Tang et al. undertook a detailed study comparing the desorption efficiencies of a variety of carbon surfaces when used as SALDI substrates [26], including multi-walled carbon nanotubes (MWNTs), buckminsterfullerene (C_{60}), nanoporous graphitic carbon [Hypercarb™] (PGC), nonporous

graphite particles (G), highly oriented pyrolytic graphite (HOPG) and nanodiamonds (ND) (Fig. 1). Although the order of desorption efficiency was found to be MWNT ~ C_{60} > PGC > G > HOPG > ND, intriguingly, this is the opposite trend to the extent of internal energy transfer: MWNT < C_{60} ~ PGC < G ~ HOPG < ND. It was concluded that increasing the extent of internal energy transfer in the SALDI process might not enhance the desorption efficiency of benzylpyridinium ions (or may lead to extensive fragmentation or degradation). The type and size of the carbon substrates was also found to be important. The authors noted that their results contrasted with those reported previously by Alimpiev et al. [27]. Specifically, HOPG and ND were found to be poor SALDI substrates, despite these surfaces being rough, and the HOPG surface required a high laser fluence to achieve laser desorption. These differences may arise because the actual substrate examined by Alimpiev was pretreated with a hyperthermal atomic beam. Further investigation revealed that parts of the carbon surfaces were laser annealed under high laser fluence and clusters of sub-μm sized spherical particles were formed (Fig. 2a). A series of carbon cluster ions (differing by *m/z* 12.0) was also observed in the negative ion mass spectra. Destruction of the surfaces of the CNTs after laser irradiation was observed, but carbon cluster ions were not seen in the mass spectrum (Fig. 2b).

Amini and Shariatgorji have also advanced the graphite SALDI technique [28–30]. Graphitised carbon black (GCB) particles embedded in a network of polytetrafluoroethylene (PTFE) were shown to be an active carbon-based SALDI substrate (Fig. 3a–c). A number of pesticides with varying chemical properties were detected (Fig. 3d), though most of the pesticides were detected as Na/K adducts or fragmented ions. The method was successfully used to determine the

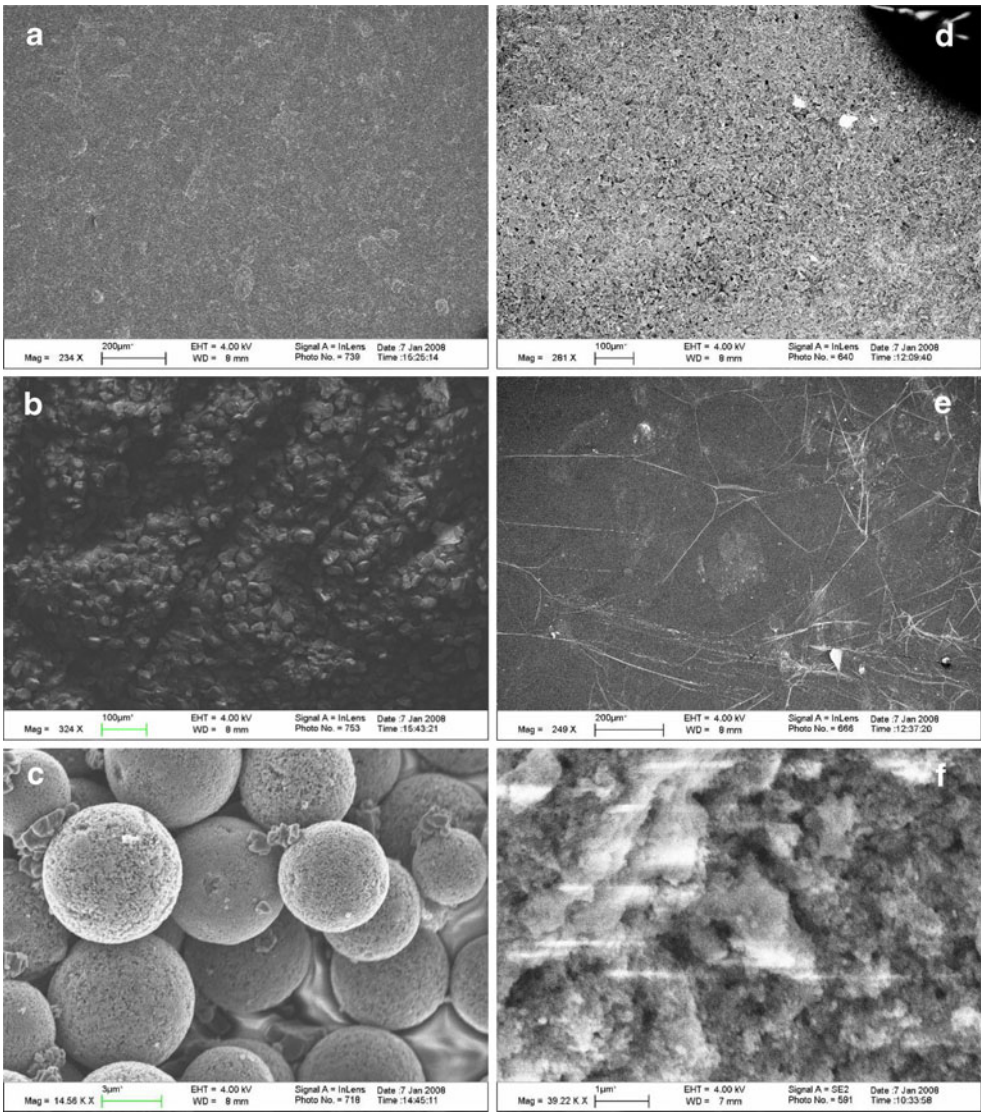

Fig. 1 **a**–**f** Scanning electron micrographs of **a** multi-walled carbon nanotubes, **b** buckminsterfullerene, **c** nanoporous graphitic carbon, **d** nonporous graphite particles, **e** highly oriented pyrolytic graphite, and **f** nanodiamonds. Reproduced with permission from [26]; copyright 2009, *Analytical Chemistry*

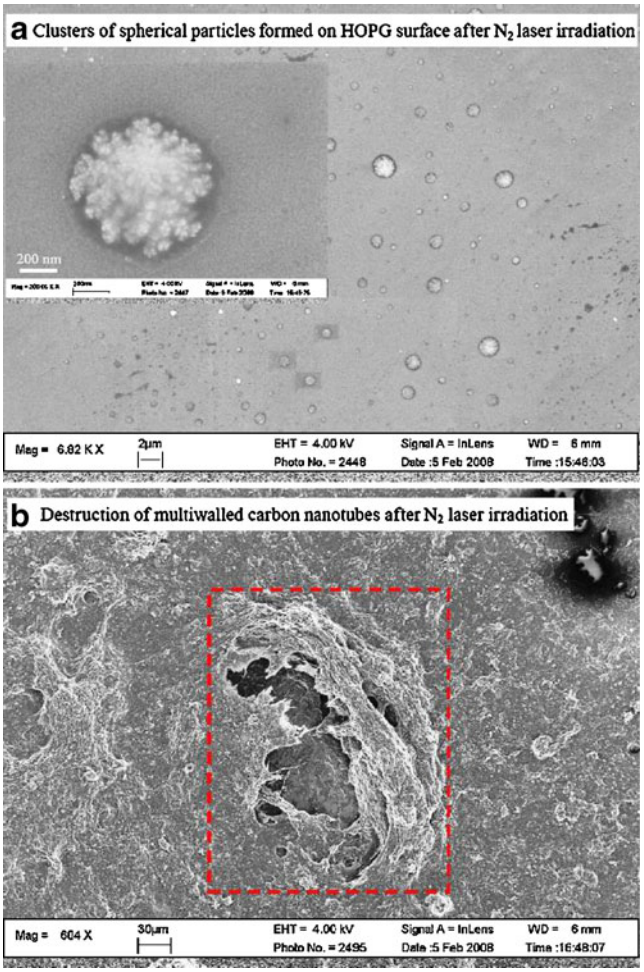

Fig. 2 **a**, **b** Scanning electron micrographs of **a** clusters of spherical particles formed on the surface of HOPG after N_2 laser irradiation (laser fluence, 109 mJ cm^{-2}) and **b** the destruction of multiwalled carbon nanotubes (CNTs) after N_2 laser irradiation (laser fluence, 43 mJ cm^{-2}). The carbon substrates were irradiated with the N_2 laser at a frequency of 10 Hz for 1000 laser pulses. Reproduced with permission from [26]; copyright 2009, *Analytical Chemistry*

presence of atrazine and one of its degradation products, atrazine-desethyl-2-hydroxy, in agricultural drainage water from rice fields [30] (Fig. 3e). Enhancement was further achieved using oxidised GCB nanoparticles, with the result being that propranolol extracted from Baltic Sea blue mussels was successfully quantified by SALDI-MS using deuterated propranolol as the internal standard [29].

The production of carbon cluster ions in carbon-based SALDI obscures the mass spectra and/or suppresses the signals of the analyte due to detector saturation. However, with the development of ion-mobility (IM) mass spectrometry, in an approach demonstrated by Ugarov et al. [31], the carbon cluster ions can be filtered out because the migration times of these ions are distinctly different from those of the biomolecules investigated. In that study, derivatised fullerene particles were chosen as the SALDI matrix and deposited on a 14 μm thick rat brain tissue slice. The tissue was then analysed directly. Figure 4 shows a representative SALDI-IM-TOF spectrum obtained before and after carbon cluster signal filtering. Although peptide and lipid ions were detected below *m*/*z* 2000, the presence of fullerene ion signals greatly suppresses their signals (Fig. 4a). However, the peptides and lipids show a distinctive trend in their IM spectroscopy compared to the C_{60} and C_{120} clusters. The fullerene ions were readily subtracted from the data (Fig. 4b), and, by combing the information generated by SALDI-MS and IM, detailed assignments of the lipid and peptide components could be made. Furthermore, IM analysis of dynorphin 1–7 was demonstrated in the same study using derivatised SWNTs as a SALDI substrate.

Nanostructured semiconductor-based SALDI

The development of SALDI-MS entered a new chapter after DIOS-MS was proposed by Siuzdak et al. in 1999 [32–34]. The innovation of DIOS-MS is its migration towards a monolithic target. By using lithographical etching (illuminating n^+-type silicon through an optical mask), or by covalent derivatisation before etching, photopatterning of the surface can be achieved. From the operator's perspective, the fundamentally different approach of the DIOS-MS lies in stark contrast to the early carbon-based SALDI approaches that are used in a manner similar to the conventional MALDI matrix. Even during the early phase of the development of DIOS-MS, it had already been noted that a wide range of biologically related small molecules could be analysed. It was thought that the porous structure of PSi provided a scaffold for trapping the analyte, and the unique optical activity of these nanostructured silicon substrates afforded an effective means of transferring the laser energy to the adsorbate [35]. PSi has been a subject of intense research effort since the early 1990s, and in-depth knowledge has been accumulated in this area [36, 37]. Much of the interest in PSi and its morphology derives from its room-temperature photoluminescent properties [38]: visible light emission from high-porosity structures arises from the quantum confinement effect. Bulk silicon, however, emits light only weakly (<0.001%) in the IR region owning to its indirect band gap [37]. Recently, on the basis that explosive vaporisation was proposed as a possible desorption mechanism, a refined version of DIOS-MS emerged, namely nanostructure-initiator mass spectrometry (NIMS) [39].

Despite the reported success of DIOS-MS, three major problems were encountered during its early phase of development. Firstly, freshly prepared hydrogen-terminated PSi is chemically unstable and a dielectric layer forms on the

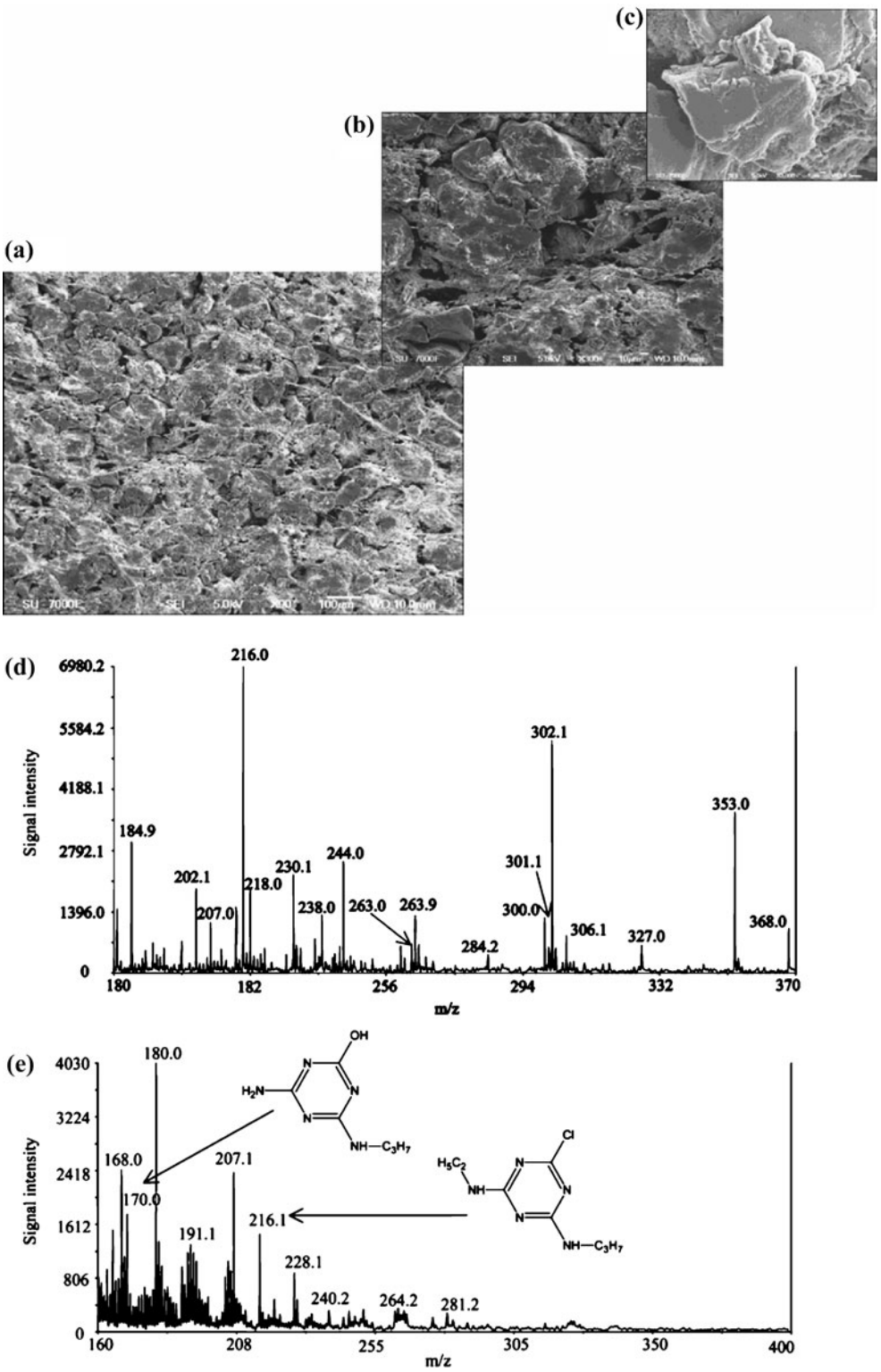

Fig. 3 **a**–**e** SEM images of a graphitized carbon black disk surface at magnifications of **a** 90×, **b** 300×, and **c** 3000×. **d** SALDI spectrum showing different pesticides retained on a GCB disk: $[methomyl + Na]^+$ (*m/z* 184.9), $[simazine + H]^+$ (*m/z* 202.1), $[atrazine + H]^+$ (*m/z* 216.0), $[propazine + H]^+$ (*m/z* 230.1), $[atrazine + Na]^+$ (*m/z* 238.0), $[carbofuran + Na]^+$ and $[chloridazon + Na]^+$ (*m/z* 244.0), $[cyanazine + Na]^+$ (*m/z* 263.0), $[parathion – methyl + H]^+$ (*m/z* 263.9), $[metazachlor + Na]^+$ (*m/z* 300.0), $[metalaxyl + Na]^+$, (*m/z* 302.1), $[metolachlor + Na]^+$ (*m/z* 306.1), $[diazinon + Na]^+$ (*m/z* 327.0), $[malathion + Na]^+$ (*m/z* 353.0), and $[azinphos - ethyl + Na]^+$ (*m/z* 368.0). **e** SALDI mass spectrum of agricultural drainage water showing atrazine (*m/z* 216.1) and one of its degradation products, atrazine-desethyl-2-hydroxy (*m/z* 170.0). Reproduced with permission from [30]; copyright 2010, *Analytical Chemistry*

surface due to oxidation. Secondly, the substrates produced by the wet chemical etching exhibit substantial inter-sample variability. Thirdly, the material has a high affinity towards hydrocarbons from ambient air and even from the residual gas within the vacuum chamber of the mass spectrometer. This leads to a characteristic chemical background in the mass spectra. These undesirable properties of PSi hindered the full potential of the material to work in SALDI-MS.

As nanomaterial science has advanced, alternative fabrication methods, chemical treatments and modifications were sought. Table 1 summarises some of the alternative approaches used to prepare nanostructured semiconductor

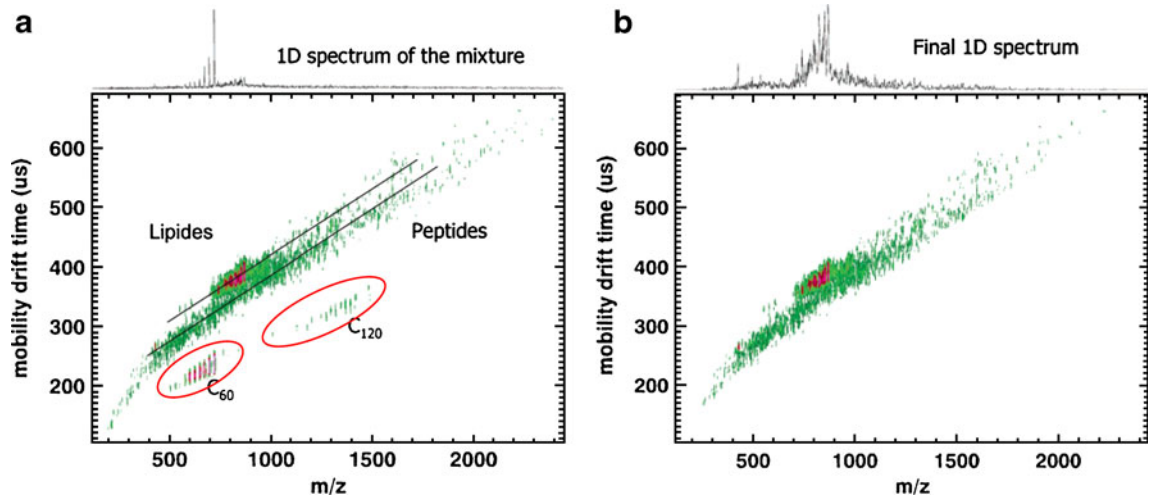

Fig. 4 **a**, **b** 2D SALDI IM-TOF MS spectra obtained from Sprague–Dawley rat brain tissue using $C_{60}((CH_2)_2COOH)_n$ matrix: **a** original spectrum; **b** the same 2D spectrum after the carbon cluster signals had been filtered out. Reproduced with permission from [31]; copyright 2004, *Analytical Chemistry*

SALDI substrates reported to date. Methods include thin-film deposition approaches, such as a nonporous column/void silicon surface produced by plasma-enhanced chemical vapour deposition (PECVD) [40, 41], germanium nanodots (GeNDs) deposited on a silicon single-crystal surface by molecular beam epitaxy (MBE) [42, 43], ordered silicon nanocavity arrays produced by reactive ion etching (RIE) [44, 45], and silicon nanowires (SiNWs) produced by chemical vapour deposition (CVD) [46–48]. These physical methods have advantages over wet chemical etching approaches, as they are carried out in computer-controlled systems ensuring the substrates produced have a high target-to-target reproducibility.

The SiNWs substrate has recently been made commercially available under the trade name of NALDI™ from Nanosys, Inc. and Bruker Daltonics, Inc. The substrates are prepared using colloidal gold nanoclusters deposited on a silicon wafer as catalysts. Nanowires are then grown using silane vapour (SiH_4) as a reactant in a CVD furnace. The SiNWs surface is further oxidised and derivatised with (pentafluorophenyl)-propyldimethylchlorosilane [46, 47]. It has been reported that the SiNWs surface exhibits significantly lower ionisation fluence thresholds than the DIOS substrate and organic MALDI matrices. SEM images also revealed that the SiNWs layer is easily melted and evaporates upon laser irradiation [47]. Important surface parameters governing the LDI performance have been further optimised and the surface morphology of the optimised substrate is different from the earlier development version reported [12] (Fig. 5). In addition, independent study has shown that the commercial NALDI™ target outperforms the commercial DIOS™ target in several aspects, particularly in low molecular weight peptide analysis [64]. However, the positive ion NALDI mass spectra have characteristic background ions located at *m/z* 197, 235 and 243, etc. [65] due to the formation of Au^+, $[AuF_2]^+$, $[AuSi(H_2O)]^+$ and other related cluster ions, and these obscure the analysis of small molecules.

Alternative chemical etching methods have also been sought. The relatively simply preparation procedure involved in chemical etching make these approaches viable in most laboratories. For example, a metal-assisted oxidative etching process termed HOME-HF etching, first proposed by Li and Bohn [66], has been explored in several studies [67–70]. This method involves an uncomplicated fabrication set up and only requires a deposition of a metal layer, such as palladium, gold or platinum, on a silicon wafer, although only the substrates prepared by Au-coating prior to HOME-HF etching were reported to be of use in SALDI. A shadow mask can be used to pattern the metal deposition and to generate an array of sample spots. Early works employed sputter coating in metal deposition, which often resulted in surface heterogeneity and the formation of "pitches" (islands of less-processed surface area) [71]. These were because of uneven Au deposition on the surface and the fluctuation of the glow discharge current during sputter coating. Subsequently, work carried out by Tsao et al. employed an e-beam evaporation approach, avoiding the problems encountered in sputter coating [69, 72]. In that study, a range of surface morphologies were produced by HOME-HF etching, but apparently a surface morphology with vertically aligned densely packed nanofilaments shows a superior performance (Fig 6a–c). Moreover, it was shown that this substrate outperformed the commercial DIOS™ target in peptide analysis.

Another similar approach that employs silver-assisted chemical etching has been reported by Piret et al. [63, 73]. In this process, crystalline silicon is etched by a solution of

Table 1 Comparison of the fabrication processes of various nanostructured and nanoparticle semiconductor SALDI substrates reported in the literature

Substrate	Summary of fabrication processes (and pre- and post-fabrication treatment, if available)	Reported year	References
Amorphous germanium oxide thin film (QuickMass™)	An amorphous Ge thin film is prepared by physical vapour deposition (PVD). Deposition/evaporation is carried out in an electron beam evaporator. The precursor material is 99.999% Ge cubes, evaporated from a vitreous carbon crucible. Corning 1737 glass and polished stainless steel can be used as the basal substrate.	2004	[10, 49]
Silicon submicrometer groove arrays	ZEP520 resists are first coated uniformly onto a Si surface. The resists on the Si substrates are exposed to an electron beam and the exposed samples are subsequently developed in ZED-N50. The resist patterns are transferred to Ni by a conventional lift-off method. The Si substrates with the Ni mold (mask) are etched by RIE using CF_4–Ar gas. The Ni mask is then removed by soaking in diluted HNO_3. The fabricated Si surfaces are refreshed by soaking in 5% HF solution and dried in vacuo.	2005	[50]
Ordered silicon nanocavity arrays	A Si wafer is first spin-coated with a positive e-beam resist, NANO poly(methyl methacrylate) (PMMA), and is then placed in an electron beam lithography system for high-resolution nanopatterning. A dried surface is then etched by reactive ion etching (RIE) in a gas mixture containing C_4F_8, SF_6 and Ar. The substrate is then treated with O_2 plasma and stored in air. Immediately prior to MS measurement, the silicon substrates are rinsed with 5% HF/EtOH to remove the residual SiO_2 layer. This method has replaced that described in [44].	2005/2009	[44, 45]
Zinc oxide nanowires	ZnO nanowires are either grown on a Si substrate by CVD or alternatively produced on an Au/Ti/Si structured substrate by a vapour transport process.	2005/2010	[11, 51, 52]
Silicon microcolumn arrays	A cleaned Si wafer is exposed to repeated 355 nm frequency-tripled Nd:YAG laser irradiations in the presence of ambient air (least active), SF_6 gas, or deionised water (most active).	2006	[53, 54]
Silicon nanopillars plus amorphous Si coating	Silica nanoparticle agglomerates are deposited as a mask produced by liquid flame spray (LFS) onto a Si surface. The surface is etched by inductively coupled SF_6/O_2 plasma, buffered in helium gas placed on a liquid nitrogen cooled bottom electrode—a method known as cryogenic deep reactive ion etching (DRIE). Subsequent development adds an α-Si coating by PECVD, either on a planar silicon surface or a surface of silicon nanopillars. The substrate can be further treated with RIE oxygen plasma treatment. Before fabrication, the Si wafer is first cleaned with a solution of $NH_4OH/H_2O_2/H_2O$. Silicon dioxide substrate is fabricated by thermal oxidation of a silicon wafer. The sample plates are stored in air inside the clean room and are cleaned by rinsing with methanol before MS measurements.	2007/2009	[55, 56]
Silicon nanoparticles	Commercially available 30 nm Si nanoparticles pretreated with 10% HNO_3 in a heated sonication water bath are derivatised with (heptadecafluoro-1,1,2,2-tetrahydrodecyl)dimethylchlorosilane (PFP). Nanoparticles are carefully cleaned throughout and applied as a conventional particulate matrix.	2007/2009	[57, 58]
Germanium nanodot chip	A Si surface is first cleaned by the standard Shiraki process, followed by pre-deposition of a silicon buffer layer to make an atomically flat and clean silicon surface. Ge atoms are deposited on the silicon surface using molecular beam epitaxy (MBE) to form a self-assembled nanoscale Ge islands. Further cleaning may be required, as described in [43].	2007	[42, 43]
Zinc oxide nanoparticles	Commercially available ZnO nanoparticles (Zn-350) are suspended in methanol and are treated by ultrasonic agitation, which leads to fragmentation and irregularly shaped nanoparticles.	2008	[59]
Ordered nanocomposite silica thin films	A freshly oxidized single crystal Si wafer is submitted to a diluted suspension of tetraethylorthosilicate (TEOS) in ethanol/water/HCl and surfactant (Brij56). The surface is then withdrawn from the solution and allowed to dry under ambient conditions. The condensation of silica precursor molecules around an organised surfactant phase leads to an evaporation-induced self-assembly process to form an ordered nanostructured silica film. The substrate is then exposed to 3 h of deep-UV light to yield a nanoporous silica thin film. Photopatterning is achieved by using an aluminium mask.	2008	[60]
Silicon nitride nanoparticles	A slurry of silicon nitride is prepared by mixing 10 mg of nanoparticles with 100 μL of 1% TFA. The slurry is then spotted directly onto a stainless steel MALDI plate and dried.	2009	[61]
Laser-assisted chemically etched porous silicon	Combines conventional electrochemical etching in HF/ethanol solution and further modified 355 nm frequency-tripled Nd:YAG laser in etching solution. The surface is carefully cleaned throughout.	2009	[62]
Chemically etched silicon nanowire arrays	A silicon surface cleaned with piranha solution is chemically etched in $HF/AgNO_3$ aqueous solution (silver-assisted chemical etching) and the substrate is subsequently derivatised with octadecyltrichlorosilane (OTS), perfluorodecyltrichlorosilane (FDTS), or octyldimethylchlorosilane (ODCS) in a dry N_2 purged glovebox after storing in an aqueous solution of $HCl/HNO_3/H_2O$ overnight. The resulting surface is rinsed with CH_2Cl_2 and isopropyl alcohol and dried under a stream of N_2.	2010	[63]

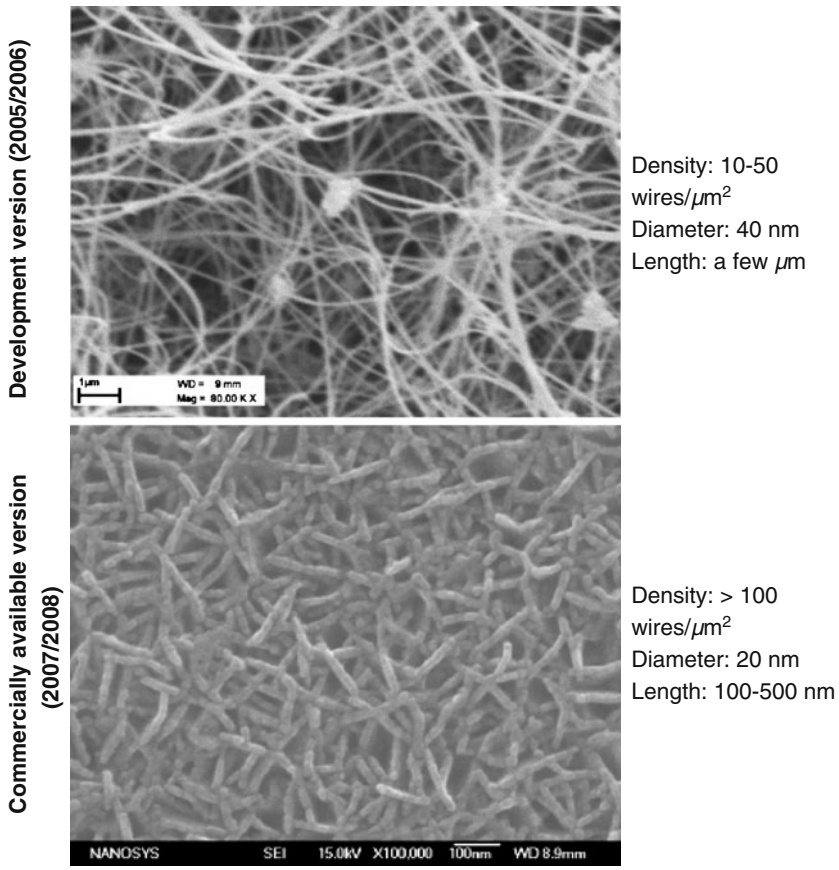

Fig. 5 Comparison of the surface morphology of the early development version and the commercially available version of the NALDI™ target. Reproduced with permission from [47]; copyright 2006, *Journal of Physical Chemistry*, from [12]; copyright 2008, *Journal of the Association for Laboratory Automation*

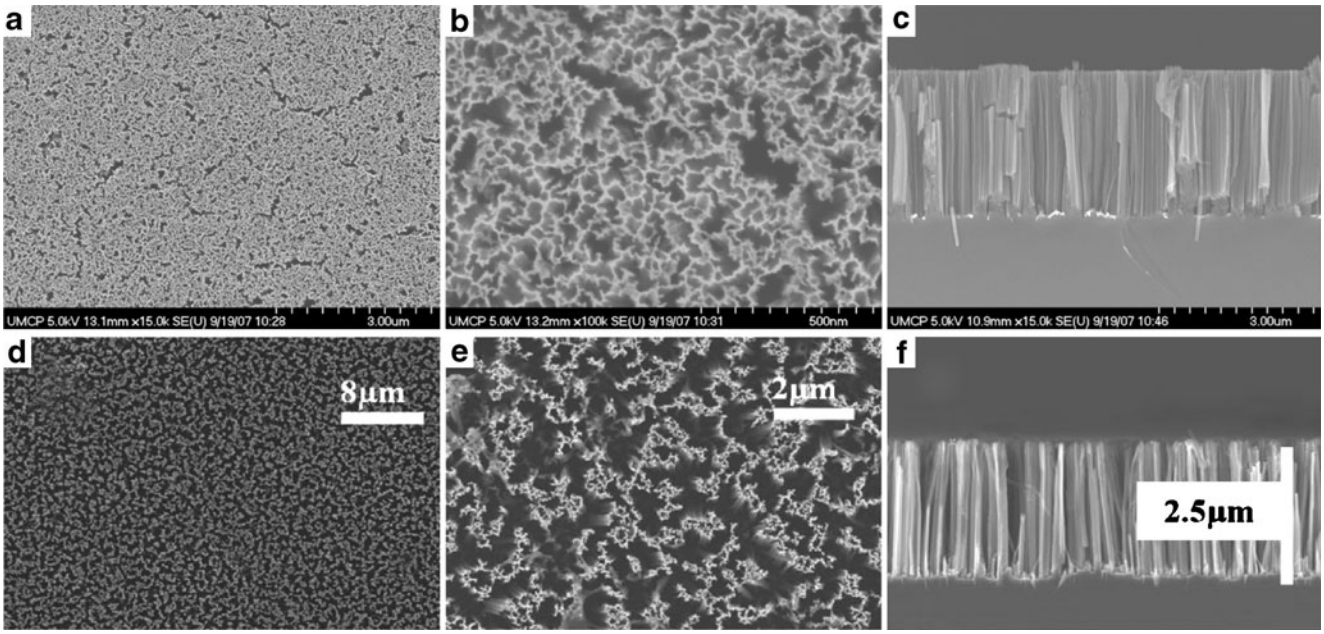

Fig. 6 **a**–**f** Comparison of the surface morphologies of **a**–**c** a nanofilament silicon substrate prepared by HOME etching and **d**–**f** silicon nanowire arrays substrate prepared by silver nitrate assisted etching. Despite being named differently, the surface morphologies of the substrates appear to be identical. Reproduced with permission from [69]; copyright 2008, *Analytical Chemistry*, and from [63]; copyright 2010, *Langmuir*

$HF/AgNO_3$. Because the surface is anodised, the silver ions are reduced to silver metal and silver nanoparticles are deposited on the surface. Therefore, the prior deposition of a metal layer (as in HOME-HF etching) is not required. However, the method requires a follow-up step to remove the silver particles and dendrites produced. The substrates reported to work in SALDI have an identical surface morphology to that reported by Taso et al., despite all of these authors naming their substrates differently (Fig. 6d–f).

In a collaboration with Vladimir Karavanskii and Sergey Nikiforov of the Prokhorov General Physics Institute of Russian Academy of Sciences, the authors explored the PSi substrate prepared by iodine-assisted etching [9]. Figure 7 shows the microscopic structures of a PSi substrate prepared by iodine-assisted vapour-phase etching. Using this method, the density of the surface nanostructures can be vastly increased compared to the conventional anodisation approach. In addition, a relatively large and uniform target can be produced. The authors' investigations of argon plasma etching [9] and an amorphous germanium thin film target (QuickMass™) [10] have also become the basis for developments relating to amorphous-Si (α-Si) thin film, as reported in [74]. The investigation of α-Si thin film was driven by the hypothesis that dangling bonds which are present in a disordered network of α-Si thin film play a fundamental role in the energy transfer mechanism.

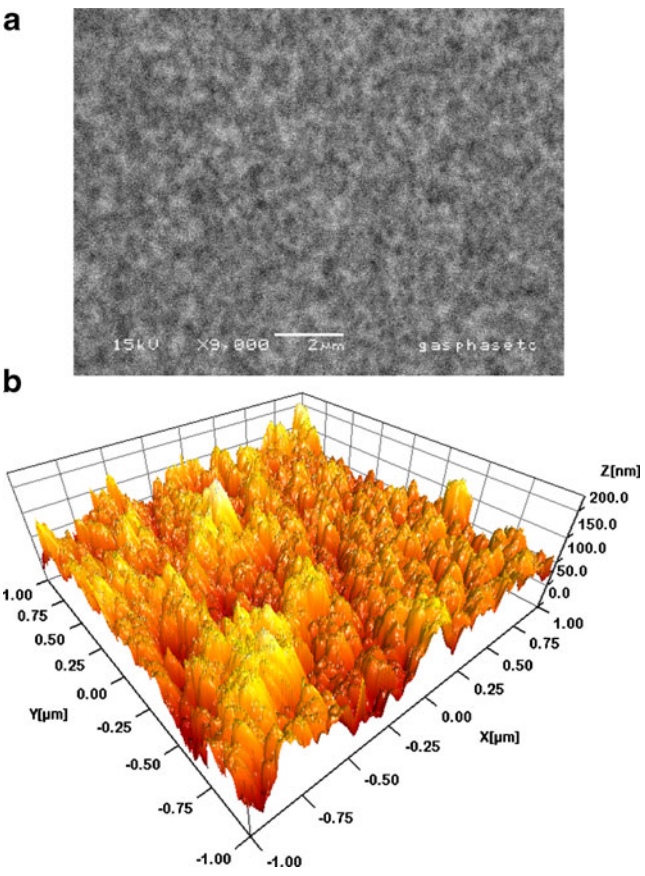

Fig. 7 **a** SEM image and **b** AFM topography of a typical PSi substrate prepared by vapour-phase etching. Etching was carried out by suspending a silicon substrate in a sealed chamber containing saturated vapours of a HF-water (1:1) solution and I_2 powder for 1 h at room temperature. No light illumination or electrical bias was required

In addition to optimising the substrate physicochemical parameters, the authors also investigated the effects of varying the ion source pressure on the DIOS performance. Increasing the ion source pressure from 10^{-6} to 10^{-3} and 1 bar produces a damping effect on the desorbed ion. The internal energy of the desorbed ions is reduced and consequently extensive metastable fragmentation or degradation can be minimised. Furthermore, because a surface or an interface is a highly dynamic system that is greatly influenced by its surrounding environment, the ion source (vapour) pressure also affects the availability of water adsorbed on the surface. The configuration of the mass spectrometer and the experimental conditions are therefore crucial factors, and may explain the inconsistent results reported in the literature. These effects are demonstrated by the DIOS mass spectra of the neuropeptides leucine–enkephalin (Fig. 8). Different mass spectral responses were observed from ultrahigh vacuum, high vacuum and atmospheric pressure (AP) systems. The protonated molecule of leucine–enkephalin and the fragment ion at *m/z* 491 dominate the AP-DIOS mass spectrum. Still, in-source decay could not be avoided. On the other hand, in all of the vacuum systems, the peak intensity of the protonated molecule was lower than its fragment and its salt adducts. In the DIOS-ToF spectrum, fragment ions at *m/z* 434 and 491 dominated. In DIOS-Q-ToF, the spectrum was dominated by the fragment ion at *m/z* 326.

SALDI ionisation mechanism on nanostructured semiconductors

The elucidation of the SALDI ionisation mechanism is possibly the most controversial and elusive area of SALDI research. The SALDI mechanism can be subdivided into adsorption, retention, radiation coupling and transfer, desorption and ionisation reactions. The physical processes that are thought to be involved in the radiation coupling reaction are described below with an emphasis on silicon substrates. Depending on the thickness of the nanostructure layer of the substrate, at least 3–4 levels of these physical processes are involved in transferring the laser energy to the adsorbate and thereby promoting them to an excited state before the desorption and ionisation reactions.

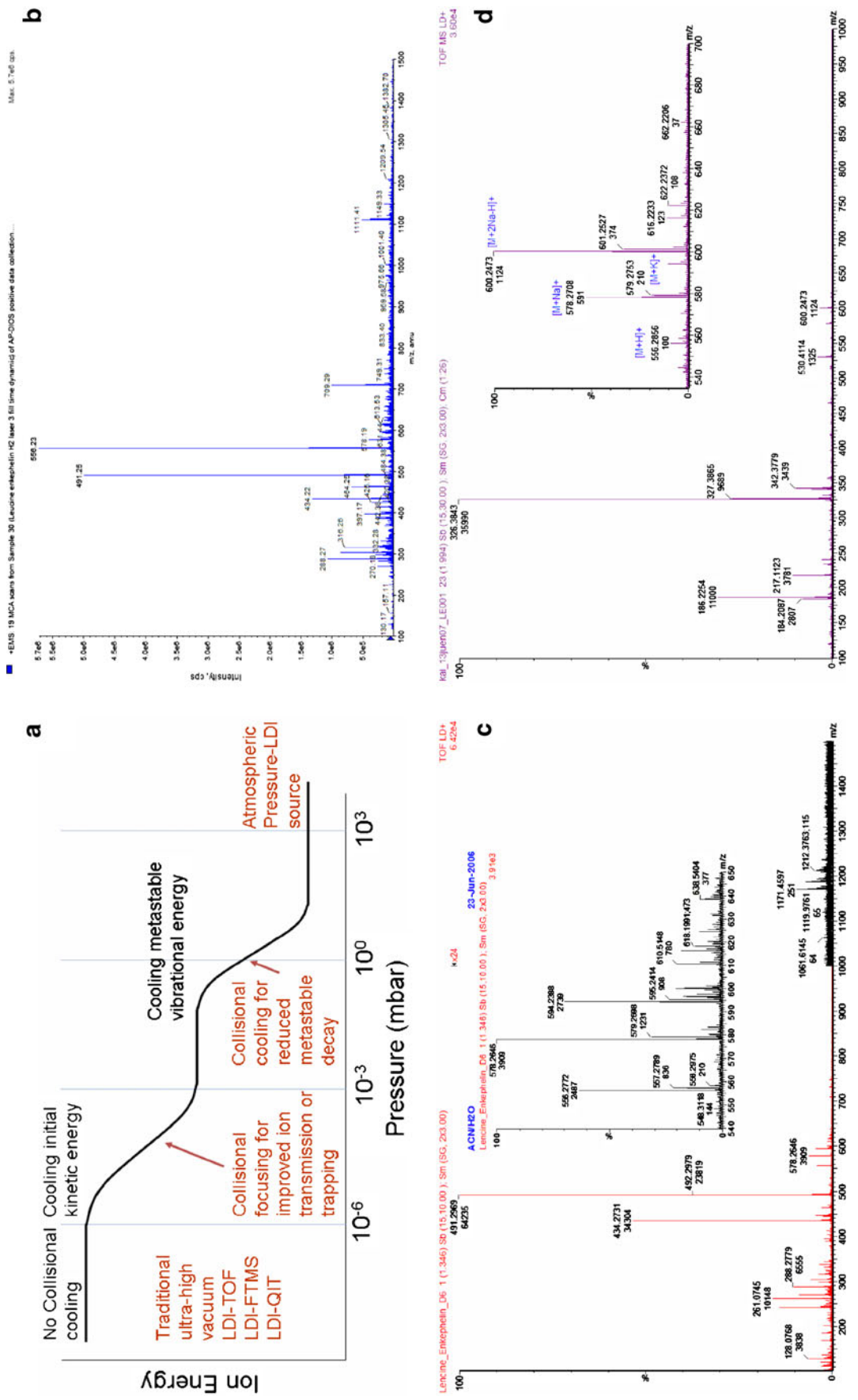
a
Ion Energy
No Collisional cooling
Cooling initial kinetic energy
Traditional ultra-high vacuum LDI-TOF LDI-FTMS LDI-QIT
Collisional focusing for improved ion transmission or trapping
Cooling metastable vibrational energy
Collisional cooling for reduced metastable decay
Atmospheric Pressure-LDI source
10-6
10-3
100
103
Pressure (mbar)
b
Intensity, cps
m/z, amu
c
d
m/z

◀ **Fig. 8** **a** The effect of ion source pressure on the relative internal energies of the desorbed ions. Also shown are positive-ion DIOS mass spectra of leucine–enkephalin acquired on **b** an atmospheric pressure-LDI-QqLIT system, **c** an ultrahigh vacuum LDI-ToF system, and **d** a high-vacuum LDI-Q-ToF system

1. Fundamental energy transfer processes

Okuno et al. noted that increasing the specific surface area of a surface, for example by sanding a silicon wafer, enabled the substrate to acquire some SALDI activity [50]. They used such substrates to obtain mass spectra of a hydrophobic polymer, reserpine and angiotensin. However, a scratched metal surface did not result in the same activity. Undoubtedly, enhancing the specific surface area will also affect the adsorption and retention of the adsorbate on the surface and the refraction of laser light. However, this observation also suggests that efficient energy transfer is achieved because of the unique electronic properties of the semiconductor surface.

In direct laser desorption, most species that are desorbed from the surface are neutral at the laser fluences required to preserve molecular integrity. Observations of how neutral molecules are desorbed from a surface have concluded that there are two main processes that contribute to the molecular desorption: (1) laser-induced *thermal* desorption (LITD) [75], and (2) *nonthermal* laser desorption induced by electronic transitions (DIET) (or more correctly, desorption induced by multiple electronic transitions: DIMET) [76]. LITD occurs through the excitation of the substrate by the creation of electron–hole pairs that relax and cause phonon excitation. On the other hand, DIET is a nonthermal process that occurs by substrate excitation, leading to low-energy electron transfer to the surface species. However, LITD and DIET alone do not lead to ion formation. The ionisation potential of a typical molecule requires 8–9 eV. The photon energy from the 337 nm N_2 laser is only 3.68 eV. Therefore, ion formation on direct laser desorption requires a substantially high laser fluence, which escalates

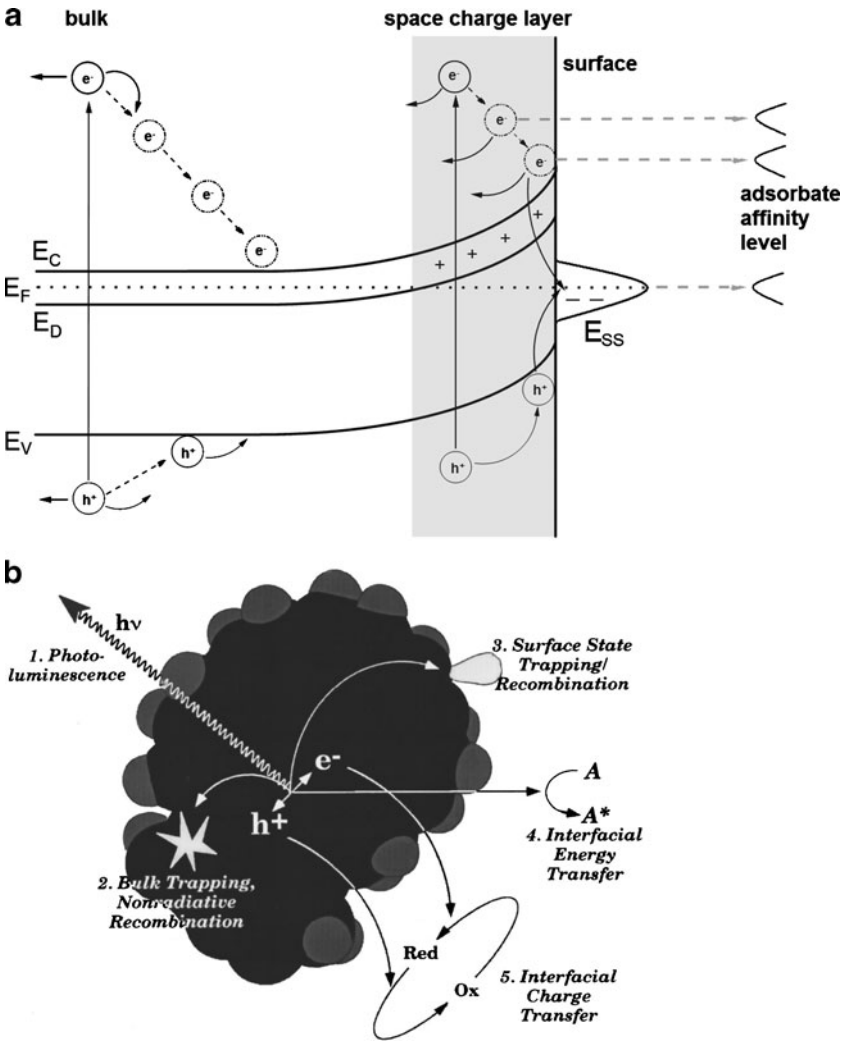

Fig. 9 **a** Schematic illustration of band bending and charge transfer on n-type semiconductor surfaces. E_C and E_V are the conduction and valence-band edges, while E_F and E_D are the Fermi energy and the energy of the bulk donor levels. Photoexcitation leads to the formation of electron–hole pairs (e^- and h^+) or excitons. Nonradiative recombination of excitons takes place at the electronic surface state (E_{SS}), which leads to the promotion of the adsorbates to an excited state. Energy thereby being concentrated to promote ionisation. Adapted from [76]. **b** Schematic illustration of photocarrier relaxation pathways available in silicon nanocrystallites. Reproduced with permission from [90]; copyright 1997, *Journal of Applied Physics*

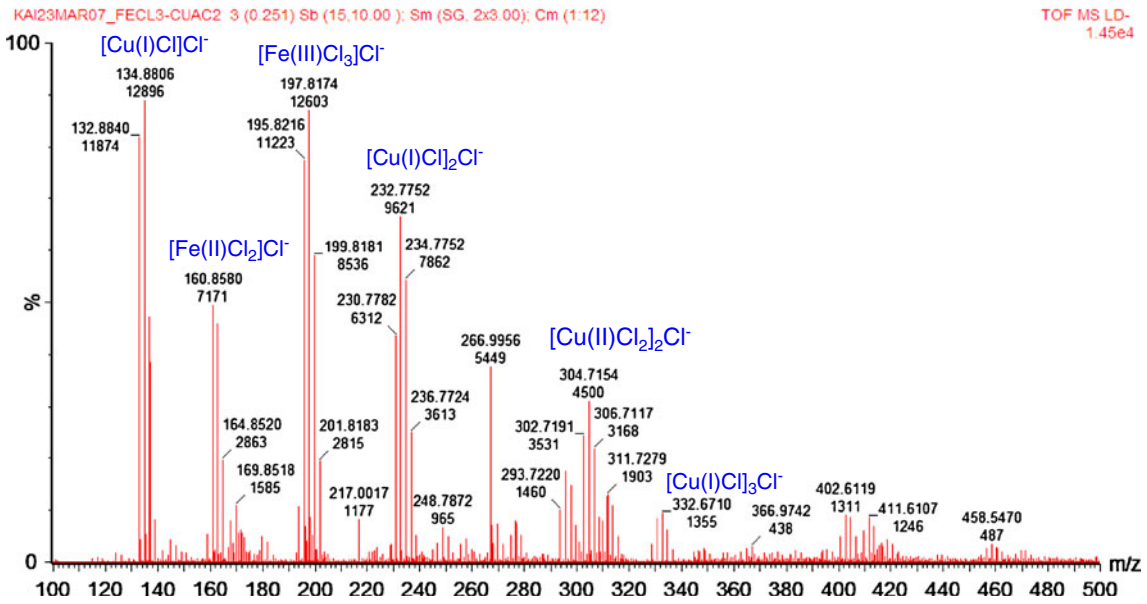

Fig. 10 Negative ion DIOS spectrum of a copper(II) acetate/iron(III) chloride mixture. Copper(II) was reduced to copper(I), and part of the iron (III) was reduced to iron(II)

the probability of multiple photons arriving at the same site simultaneously, and thereby inducing fragmentation and degradation of the adsorbate. An important concept in MALDI ionisation is photoexcitation and energy pooling. Energy pooling is one of several energy concentration possibilities imagined in early MALDI work. This is a phenomenon in which the electronic excitation energy of two nearby molecules is redistributed and higher energy processes become possible [77, 78]. It is thought that the unique electronic structure of a semiconductor surface allows the possibility of energy pooling.

Whilst charge-transfer excitation on metal and semiconductor surfaces involves initial photon adsorption by the substrate, the detailed mechanisms differ significantly for the two surfaces. The charge-transfer dynamics on a semiconductor surface are governed mainly by the band structure; principally the presence of a space-charge layer. Figure 9A illustrates a simplified schematic of a charge-transfer photoexcitation process on an n-type semiconductor surface. A space-charge layer occurs because the electronic configuration of the surface atoms is different from the bulk. All atoms in the bulk of a pure metal or elemental semiconductor are equivalent. However, the atoms at the surface do not possess their full complement of bonding partners [79]. Consequently, a semiconductor surface usually possesses electronic surface states and such states are energetically located in the band gap [76]. These relatively localised states can result from dangling bonds on the surface, or from defects or impurities. Depending on the type of surface state (donors or acceptors) and the position of the Fermi level at the surface, the surface states may carry charge, which is screened by an opposite charge inside the semiconductor material. Due to the low free-carrier concentration in semiconductors, the screening length is long and a space-charge layer is formed, giving rise to band bending [76].

When photons with energies that are larger than the band gap are absorbed by the surface, electrons from the lower band can be promoted to the upper band, and this creates energetic electron–hole pairs or excitons. Within the space-charge layer, electron–hole pairs are driven apart by the space-charge field. For n-type semiconductors, electrons are driven into the bulk, while holes are transported toward the surface. This is because the charged carriers (electrons and holes) are separated by the surface band bending, thereby producing UV radiation mediated surface oxidation [80]. The oxidation of silicon induces a reduction potential of –0.91 eV, which is sufficient to reduce, for example, Cu(II) and Fe(III) to Cu(I) and Fe(II), respectively [81–84] (Fig. 10). When such charge separation or exciton formation creates an electric field, and when it is relaxed via nonradiative recombination of electrons and holes or carrier–phonon scattering, this causes an electronic perturbation and vibrational excitation of the surface and adsorbates.

Without the band bending and the electronic surface state, the photoexcited electrons would quickly settle into the energy minimum of the conduction band. This is because of the momentum difference between the energy minimum of the conduction band and the energy maximum of the valance band in indirect band-gap semiconductors. Consequently, *non*radiative recombination of electrons and holes is prohibited, and efficient excitation of the adsorbates does not occur. Hence, for a surface composed of pure

silicon, which does not have a thick layer of nanostructures or nanocrystallites, and has its surface dangling bonds hydrogenated and its defect density significantly reduced by hydrogen plasma (e.g. α-Si–H) [85], the SALDI activity would be quenched [74]. Then again, substrates that consist of different materials may not share an identical excitation pathway. Graphite, for example, has a negative indirect bandgap—the energy maximum of the valence band is higher than the energy minimum of the conduction band—and so it may not have an identical excitation pathway to that of silicon or germanium.

2. Optical absorption (photonic and electronic band gaps)

Although surface dangling bonds or defects play an important role in the SALDI mechanism, the fundamental processes described above are initiated by the absorption of photons. Nonetheless, most of the UV photons are reflected from a rough surface or penetrate through a thin film surface. This contrasts with high-porosity surfaces, which have high optical absorbance over UV wavelengths and appear dark visually. Nayak and Knapp have correctly pointed out that this distinct optical absorption is due to the photonic band gap behaviour of nanoporous surfaces, which behave as photonic crystals [86]. Since the photonic band gap behaviour is a function of the pore lattice spacing, varying the width and depth (or generally the overall porosity) of a porous surface may change the photonic band gap behaviour, resulting in a shift in the absorption maxima, which affects the SALDI activity. This proposition is coherent with the observation that was previously reported by Okuno et al. [50] that SALDI from grooved surfaces is a function of the irradiation angle, i.e. laser irradiation normal to the grooves yields a good LDI signal, whereas parallel irradiation gives a poor LDI signal, along with other experimental evidence [87–89]. This proposition is also consistent with the experimental results reported in [45]. Still, the effects of the porosity of a substrate are not just limited to radiation absorption; it also affects the adsorption, retention and desorption of the adsorbate and residual solvent, and the thermal conductivity of the substrate, thereby attenuating the overall SALDI responses of a nanoporous substrate.

Although nanophotonic behaviour provides important insight into how optical absorption events may occur on nanoporous surfaces, an electronic event must follow in order to transfer the laser energy into internal energy. It has long been proposed that a common optical absorption event is necessary for the DIOS activity and the photoluminescence of the PSi, although both processes can occur independently [67]. This contributes to the unique electronic properties of the silicon nanocrystallites on the PSi surface [90]. The electronic structure of silicon is altered on the nanoscale and the calculated band gap is reduced to 0.65–0.25 eV, depending on the lattice symmetry [91]. In agreement with the calculated values, experimental measurements using a time-of-flight electron spectrometer have also shown that the band gap energies of nanosized Si clusters (Si_{11}, Si_{14}, Si_{17}, Si_{18}, Si_{30}, Si_{33}) are on the order of 0.4–0.6 eV [92]. However, the role of the nanocrystallites is not limited to acting as an absorption body for laser radiation; they also amplify all of the fundamental processes described above (Fig. 9B).

3. Thermoelectric effect

The reduced thermal conductivity and field effect of nanostructured substrates have both long been proposed to be important elements in the SALDI mechanism. The field effect was once suggested to be a sharp-tip electrostatic [27] or an (inverted) lightning-rod phenomenon [44], despite the lightning-rod effect occurring when the particle is off-resonance, providing only a very small amplitude enhancement [93]. Conversely, surface melting has been thought to play a critical role in the SALDI mechanism [9, 10, 94, 95]. The underlying physical process is probably the thermoelectric effect. This process is the direct conversion of a temperature gradient to electric voltage and vice versa, and it is pronounced on substrates that have a thick porous or nanowire layer and have critical dimensions or spacings below 300 nm. It is believed that laser irradiation induces rapid heating on the top of the nanowire layer. An extreme temperature results, which melts the surface, but the actual melting temperature is hundreds of degrees lower than the melting point of the bulk materials (crystalline silicon: 1410 °C; platinum: 1768 °C) due to melting-point depression. However, owing to the large difference in mean free-path lengths between electrons and phonons, electrons are driven toward the cooler bottom layer—the bulk of the substrate and the basal support—leaving the positive holes on the top layer. However, recombination of the charge carriers only occurs at thermal equilibrium, which is only slowly attained. A very high electric field is generated. Energy is transferred to the adsorbates via processes similar to that of field ionisation, in conjunction with the thermal processes already in place. As shown by the authors previously [10], this process was disrupted as the laser energy was increased beyond an optimal point. This was partly because the surface and the surface nanocrystallites were ablated and destroyed, and partly because the laser radiation was sufficiently intense to penetrate deep into the substrate, disturbing the thermal gradient. As a result, the thermoelectric effect was quenched.

4. Desorption

A thermal process known as explosive vaporisation has also been proposed as a possible *desorption* mechanism on porous substrates [96–98]. Explosive vaporisation occurs when a liquid is heated so rapidly that density fluctuations

in the liquid become the dominant vaporisation mechanism, rather than heterogeneous nucleation. Heterogeneous nucleation takes place when the temperature of the bulk liquid approaches saturation temperature and thus reaches equilibrium with its vapour. In contrast, explosive vaporisation occurs when the liquid approaches a region of intrinsic instability because its temperature gets too close to the superheat limit [99]. Indeed, when a fluid is confined to a very small cavity that is close to being molecular sized, its phase behaviour is altered. Long-range fluctuation and thermal–vibrational effects could provide another energy-transfer pathway. Nevertheless, molecular dynamics and interfacial interactions in a confined space remain less well understood and can only be studied by neutron scattering [100–103].

5. Ionisation

Depending on the chemical properties of the analyte molecules, several possible ionisation reactions follow. These include excited-state proton transfer, disproportionation reactions, fragmentation reactions, ion-molecular reactions, cation attachment or transfer, etc.

In excited-state proton transfer, the surface Si-OH moieties play a critical role in the proton transfer reaction, as evidenced in [9, 74]. Surface melting, which also increases the bond distances of the lattice system, is also implied to facilitate the protonation reaction, especially for compounds such as amines that form complexes with the surface Si-OH moieties [10, 74]. The theoretical basis that interfacial water and Si-OH terminals are the major proton sources, but not the Si-H groups (as some have proposed), has also been described in [104].

A close inspection of the SALDI mass spectra of amines acquired from a reflector ToF mass analyser often reveal a tailing region of the molecular ion peak. This phenomenon is due to the metastable states of desorbed ions. Metastable peaks are result from fragmentations that occur in the field-free region of the spectrometer (i.e. while passing down the flight tube). Fragment ions are lost by the reflector due to their change in kinetic energy. Only fragments that still have kinetic energies close to that of the precursor, such as $[M+H\text{-}NH_3]^+$, are transmitted, due to the energy tolerance of the reflector, and this gives rise to a "tailing" of the signal. However, in linear ToF systems, the intensity of a molecular ion signal does not reduce, because the linear velocity of the fragmenting ion is conserved and the fragments formed are therefore detected at the same flight time as their intact precursor. The internal energy of the excited molecules is redistributed via intramolecular vibrational energy redistribution (IVR) [105]. The energy is randomly distributed over the molecule and becomes concentrated in particular ways which in turn give rise to unimolecular reconfiguration and dissociation [106], obeying the principles of quasi-equilibrium theory (QET) [107]. This may explain the ordered fragmentation often observed. Indeed, the relatively controlled and specific fragmentation pattern and its application for post-source decay (PSD) in DIOS, similar to that of MALDI, is an unusual capability of the technique that is worth paying attention to [32, 35, 108, 109].

Gas-phase secondary ion-molecular reactions can also occur and give rise to products of cation attachment and alkylation. As an additional note, ionisation reactions in SALDI or MALDI are chemical processes and, like any chemical reactions, are governed by the principles of thermodynamics. Accordingly, it is the *entropy of the reaction which ultimately determines the ionic species detected by the mass spectrometer, while the rate of reaction determines the selectivity.*

Chemical and biomedical applications

Over the years, a large number of works demonstrating the versatility of the SALDI technique have been reported, and these were reviewed previously by Peterson [6]. The applications reported range from novel pharmaceutical and biomedical applications to environmental and polymer sciences. Of all these SALDI techniques, DIOS has been the most widely used. For example, DIOS has been shown to be a powerful tool for the forensic investigation of contraceptive polymers in an alleged sexual assault case, and it produced evidence that would not have been otherwise made available to the prosecution by another analytical technique [110, 111]. It has also been shown that the technique is highly desirable for the forensic analysis of illicit drugs [112]. In that report, despite the presence of "matrix constituents" in the "authentic" sample (e.g. ecstasy tablets seized by the police), the authors reported that interference was not observed. However, another report described that 11 impurities were identified in ecstasy by DIOS, depending on the synthetic route employed [113]. It was suggested that profiling the impurities might provide information on their origin. These authors also reported the identification of catecholamines (dopamine and noradrenaline) in a human peripheral blood lymphocyte extract [114], reconfirming the result published by the same group eight years earlier [115]. Okuno and Wada have also demonstrated the quantitation of salicylate in human serum using DIOS-MS in negative ion mode [116]. An ordered nanocavity silicon SALDI substrate was also used to monitor osmotically induced fluctuations in plant metabolites in both wild-type and transgenic *Arabidopsis thaliana* (the transgenic was modified with a human inositol polyphosphate-5-phosphatase enzyme) under the environmental stress of

drought. Root, shoot and leaf extracts were studied [44, 117]. On the other hand, there has been a great deal of interest in using DIOS-MS in bottom-up and middle-down proteomics, for example to enhance the confidence in protein identification by extending the additional information window in the low-mass region of the mass spectrum, to detect peptide peaks that cannot be detected by MALDI, and to identify post-translation modifications that can only be detected by DIOS [46, 70, 97, 118–122]. Further selected applications highlighting the strength and uniqueness of the SALDI technique are discussed in this section.

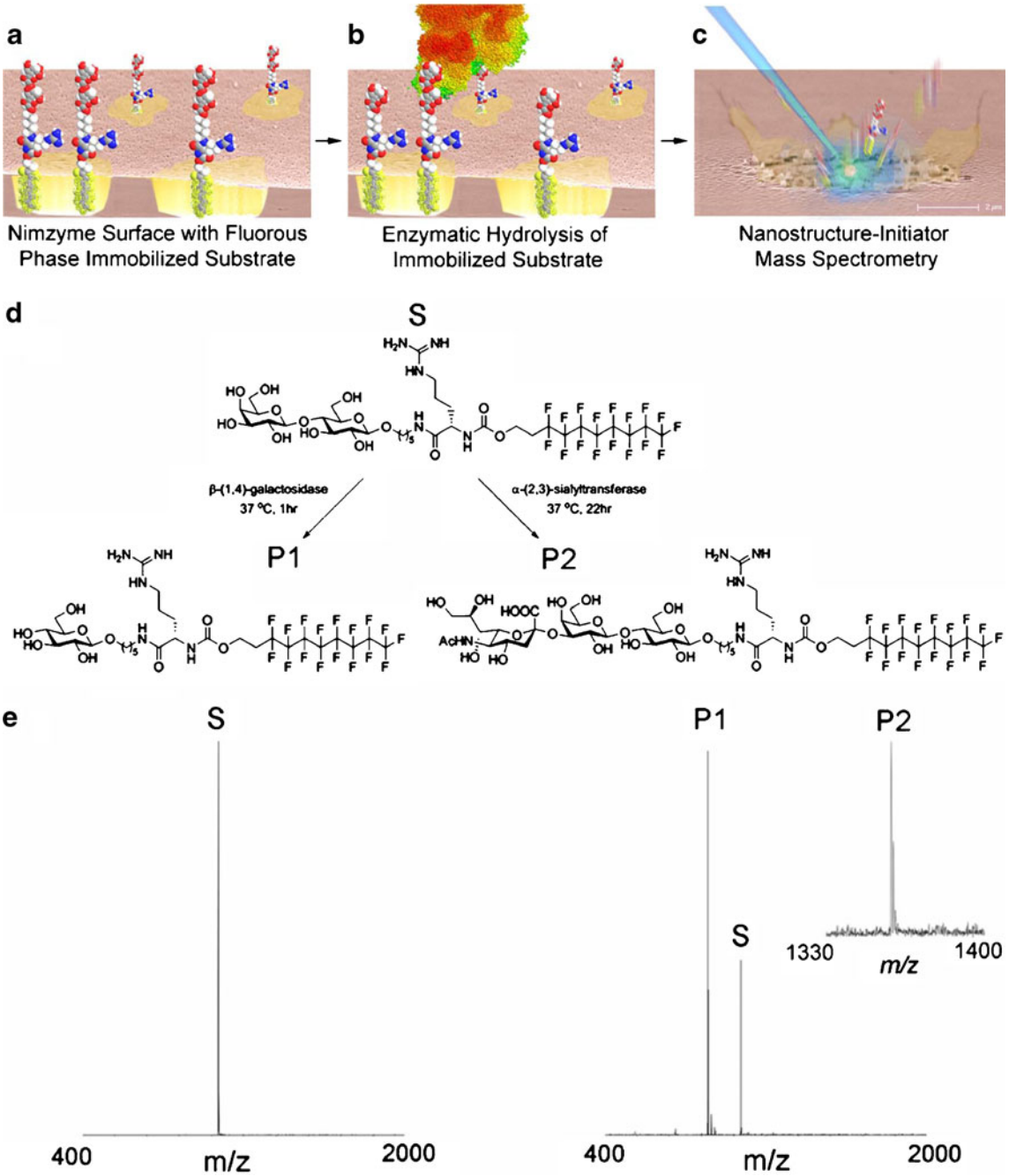

Fig. 11 **a**, **e** Schematic of an on-chip NIMS enzymatic assay. **a** The fluorinated tagged metabolite is first immobilised in the fluorous initiator liquid phase coated on the surface. **b** The surface with the sample to screen for enzymatic activity is then incubated. **c** After an on-target sample clean-up, the target is then submitted to laser mass spectrometry analysis. **d** The chemical structure of the fluorinated tagged substrate (S, $[M+H]^+$ *m/z* 1,074.30) and the products of β-1,4-galactosidase (P1, $[M+H]^+$ *m/z* 911.24) and α-2,3-sialyltransferase (P2, $[M+H]^+$ *m/z* 1,365.40). **e** Mass spectra of the substrate (*left*) and the resulting products (*right*). Reproduced with permission from [127]; copyright 2009, National Academy of Sciences (USA)

Monitoring enzymatic activity and enzyme inhibitor assay

On-target enzyme-catalysed reaction monitoring and direct analysis by DIOS-MS was first reported by Thomas et al. [119]. A number of enzyme systems were investigated. For instance, acetylcholine esterase (AChE) was allowed to react with its naturally occurring substrate acetylcholine to produce choline. MALDI and ESI were also employed for comparison, but neither was found to produce a strong, reproducible signal for choline. The lack of a strong chromophore on choline (and possibly other unadorned natural substrates) also made absorption or emission techniques difficult to employ. However, no technical problem was encountered when using DIOS-MS, and they reported that the presence of the enzyme on the surface (in the concentration range investigated) did not interfere with the detection of the small molecules of interest. The strength of this approach was further demonstrated by its ability to directly determine the selectivities of enzyme inhibitors. Three different inhibitors of AChE (huperzine A, tacrine and 2,6-dimethoxyphenyl-*N*-butylcarbamate) were studied, and the inhibition potentials of the inhibitors were found to correlate with their relative K_i values. Further comments can be found in [123].

Despite the fact that on-target enzyme activity and inhibitor assay offers a wide range of advantages, the on-target approach was abandoned in favour of an off-line approach in subsequent studies [124–126], until further work was reported by Northen et al. [127]. This was achieved after substantial effort had been invested in the development of NIMS [39] and the development of a selective on-target sample enrichment and clean-up method: fluorous affinity tagging [108]. This new approach took advantage of the fact that perfluorinated tagged components have a strong affinity toward the perfluorinated liquid initiator coated on the surface and are noncovalently immobilised. This factor is apparently a key consideration for their subsequent mass analysis because of the difficulties encountered in using covalent linker approaches previously. A biological matrix, such as a cell lysate, which contains the enzyme being investigated is then added to the surface and allowed to react with its corresponding substrate. Because the fluorous-tagged reactant and products are preferentially retained, this allows the use of surface washing steps to remove all other unlabelled components and cellular materials. This approach not only eliminates the prior purification of the enzyme from a complex biological sample as well as the subsequent quenching step required in the previous studies, but it also allows the resulting mass spectra to be free of interferences and/or ion suppression (Fig. 11). However, since the reactant is partly immobilised on the surface, which may hinder the binding of the substrate to the enzyme, careful

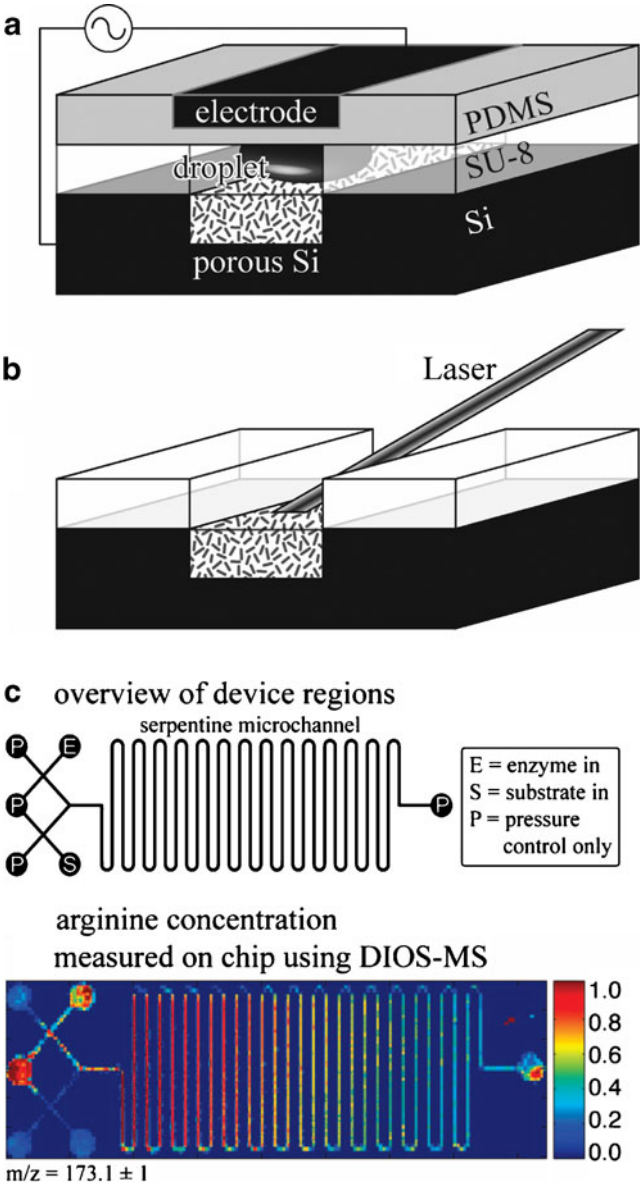

Fig. 12 **a** Cross-section of a PSi kinetic analysis microfluidic device. A droplet travels down the channel, depositing reaction product on the channel walls. **b** The deposited reaction product is then desorbed and ionised according to the principles of DIOS-MS. **c** An overview of the regions of the device and a DIOS-IMS image of arginine (*m/z* 173.1±1) over the device after an enzymatic reaction has taken place within it. Intensity correlates with relative concentration. Reproduced with permission from [128]; copyright 2008, *Analytical Chemistry*

experimental design must be implemented to permit this method to work effectively. In their study, a five-carbon linker was introduced between the tagging and substrate to reduce steric hindrance for enzyme binding, and arginine was incorporated to facilitate ionisation (Fig. 11d). This system was then applied to study the β-1,4-galactosidase activity of bacteria that were found to colonise in the near vicinity of a hot spring in the Yellowstone National Park. The results showed that the bacterial galactosidase is most

active at a temperature of 65 °C but retains its activity at even 100 °C. In addition, despite the bacteria being collected from a slightly alkaline environment, the bacterial galactosidase activity was optimal at pH 5.5, suggesting that the intracellular pH was different from that of the surroundings of the bacteria. Deoxygalactonojirimycin was also found to have a stronger inhibitory effect on galactosidase than phenylethyl-β-D-thiogalactopyranoside does.

A limitation of the approaches described above is that they can only be applied to enzyme systems which have a relatively low or moderate reaction rate. Improvements to allow time-resolved kinetic analysis for moderately fast reaction systems were reported by Nichols et al. [128]. They used an integrated microfluidic system with a PSi microchannel to perform a chemical reaction in a continuous flow regime and an in-line investigation of product formation by DIOS-MS in order to study an arginase system. The basic idea of the microfluidic system is that the device first mixes an enzyme droplet and a substrate droplet. This combined enzyme/substrate droplet then travels down a PSi microfluidic channel, depositing a trace amount of reaction substrate and product into the silicon pore walls. Because the pore size is tuned to be larger than the substrate and product, but smaller than the mean diameter of the enzyme, the enzyme is therefore sterically hindered from entering the pores. This not only allows continuous substrate diffusion into the pores and the reaction to continue down the line, but it also eliminates the need for quenching. The flow rate of the liquid droplets, or in this case the distance they travelled through the microchannel network, represents the time domain of the reaction. The whole device is then submitted to imaging mass spectrometry, and the relative concentrations of the reactant and product are monitored with respect to the position (Fig. 12). The most obvious advantage of such a device is being able to rapidly obtain enzyme initial velocity measurements, and because the entire surface of the microchannel is analysed using DIOS-MS, there is nearly zero dead time.

Pharmaceutical development

One of the most challenging areas of drug development is the search for novel receptor–ligand pairs and enzyme inhibitors, as many novel proteins have no known binding partners. Zou et al. have demonstrated an innovative approach using DIOS to address this challenge [129]. They immobilised a targeted protein (BSA) on a PSi surface that acted as a probe. A mixture of drug molecules that contained possible binding partners to the protein was then incubated with the probe. The drug molecules that have a high affinity for the targeted protein were captured by the immobilised protein, and those with a weak affinity for the targeted protein were washed off. The captured drug molecules were then identified by means of on-probe SALDI analysis. This method offers high-throughput screening of lead-drug candidates, but—unlike the conventional methods—it does not require fluorescence or chemiluminescence tags (note: labelling molecules can sometimes alter the binding affinity), radioactive markers, or even prior purification. It is not limited to immobilising protein on the probe; the method could potentially be extended to other biological macromolecules, such as DNA and RNA. The method was developed further in a subsequent study after a silicon–carbon surface attachment method was realised in which PSi substrates were chemically modified to yield carboxylic acid terminated surfaces, allowing proteins to be covalently attached to the surface through an amide bond [130]. A hemoglobin-modified surface was applied to identify the noncovalent binding between hemoglobin and 13 environmentally relevant chemicals, including antimicrobials, insecticides, fungicides and herbicides. In all of the compounds investigated, only triphenyltin chloride was shown to bind haemoglobin strongly, indicating that it may have a higher toxicity than the other compounds tested. Then again, the immobilisation of typsin on a DIOS substrate for enzymatic activity and inhibitor assay, although possible, was not as promising [131]. Immobilisation of the enzyme resulted in a slight loss of its catalytic activity and the value of ν_{max} was found to be lower than that of free trypsin. Furthermore, because of the surface chemical modification, the substrate exhibited a lower SALDI activity, and the addition of organic matrix was required to successfully desorb the peptide fragments generated.

Biochemical evolution

Ribose molecules form the backbone structure of DNA and RNA. The borate ion is thought to play an important role in the synthesis of ribose and other pentoses from simple organic precursors such as formaldehyde and glycolaldehyde which have been identified in star-forming regions of interstellar medium [132, 133]. It is thought that glycolaldehyde may have a role to play in the origins of life in our universe, and the reaction is thought to occur on or under the surfaces of tiny dust grains, initiated by a shock wave of energy. One important question in the evolution of ribonucleic acids is why ribose was favoured over other pentose isomers. Using the DIOS technique, an attempt was made by Li et al. to answer this question [68]. The actual study was performed to quantify the relative tendencies of ribose, lyxose, arabinose and xylose to form a borate-centred pentose dimer on the surface or in the gas phase, in a combination of conditions similar to that of the interstellar medium. The results showed that ribose

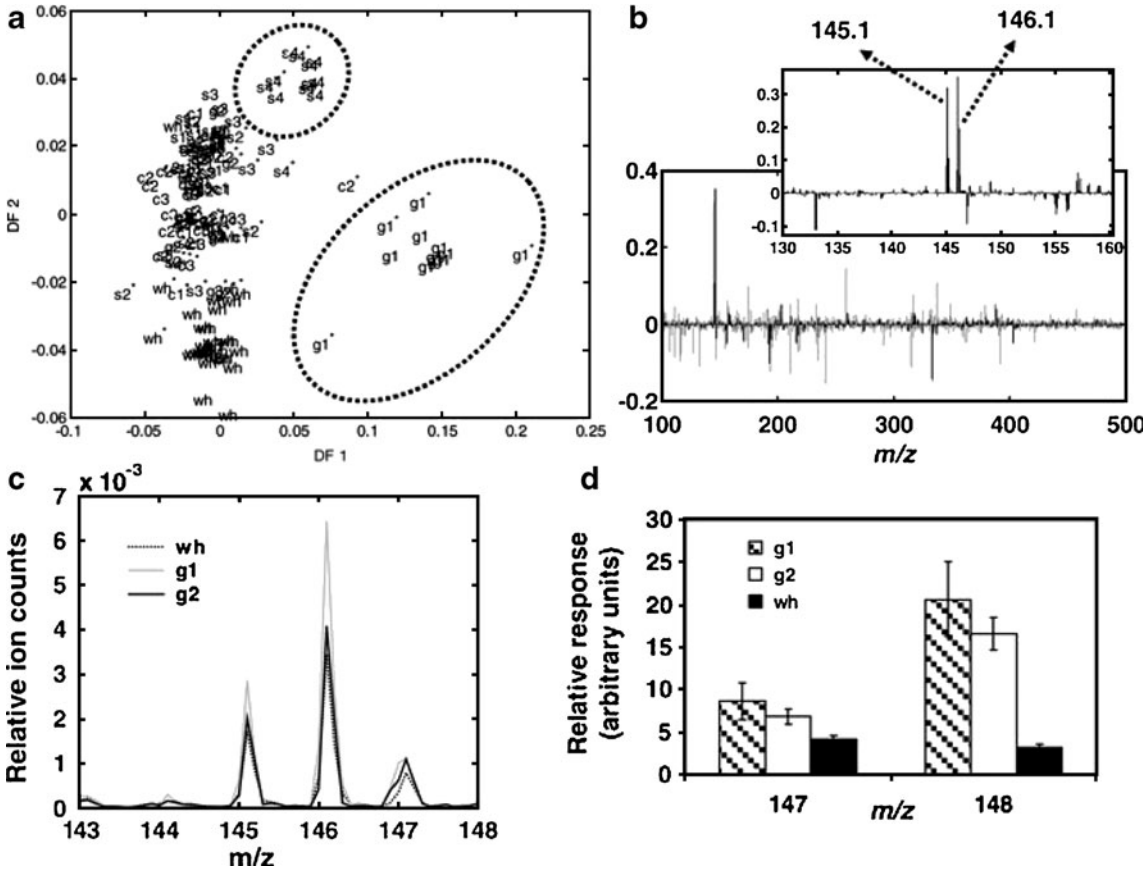

Fig. 13 **a** PC-DFA score plot constructed using the first 60 PCs, showing the discrimination of mutants g1 and s4 from the other yeast mutants and the wild-type strain. The test set is marked with an *asterisk*, and the separating clusters are *encircled* for clarification. **b** The first loadings plot of the PC-DFA. Note the prominent peaks at *m/z* 145 and 146, seen clearly in the expanded portion of the loadings. **c** Mean spectra of g1 (gln3Δ), g5 (dal80Δ) and the wild-type wh (BY4741) strains, showing the differences in the spectra in the region where the prominent discriminatory effect is observed. Note the higher peak intensity at *m/z* 146 (corresponding to glutamate, $[M\text{-}H]^-$) for g1 compared to the rest. **d** Mean spectral responses corresponding to glutamine (*m/z* 147) and glutamate (*m/z* 148) in the positive-ion direct infusion mass spectra of the three strains in **c** (*error bars* represent one standard deviation about the mean). Reproduced with permission from [134]; copyright 2005, *Metabolomics*

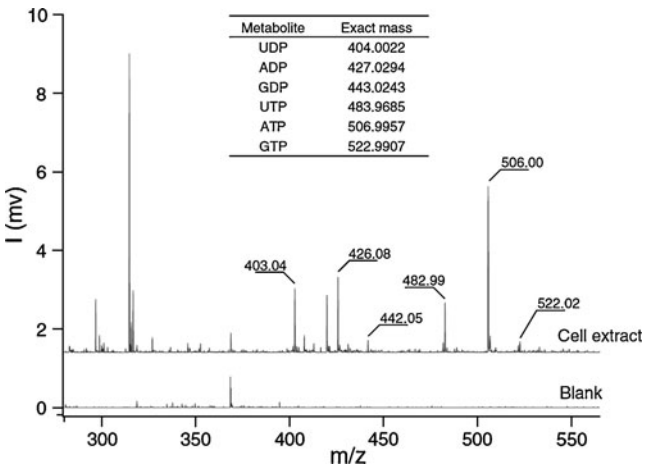

Fig. 14 Negative-ion NIMS spectra of 1 μl of a yeast cell extract and of water (blank) using 3-aminopropyldimethylethoxysilane initiator. Identified deprotonated ions of phosphorylated nucleotides are labelled, and their corresponding exact masses (as neutral compounds) are given in the inserted table. Reproduced with permission from [136]; copyright 2009, *Metabolomics*

exhibits a higher affinity to boron than other isomeric pentoses do. The resulting enrichment could provide insight into why ribose was favoured as a building block in RNA evolution.

Metabolic profiling

With the increasing interest in metabolomics over the last decade, SALDI-MS and other novel ionisation techniques—collectively known as direct analysis mass spectrometry (DAMS)—are becoming attractive alternatives or complementary approaches in metabolomics. Goodacre et al. were the first to demonstrate that metabolic footprinting (metab-

Fig. 15 **a**, **b** A PCA model based on metabolite profiles of methanol/chloroform plasma extracts collected from patients and controls. **a** PCA score plot of metabolite profiles from patients who suffered from polycystic ovarian syndrome. The patient group is labelled "P" and the control group is labelled "C". **b** PCA loading plot corresponding to the score plot shown in **a**

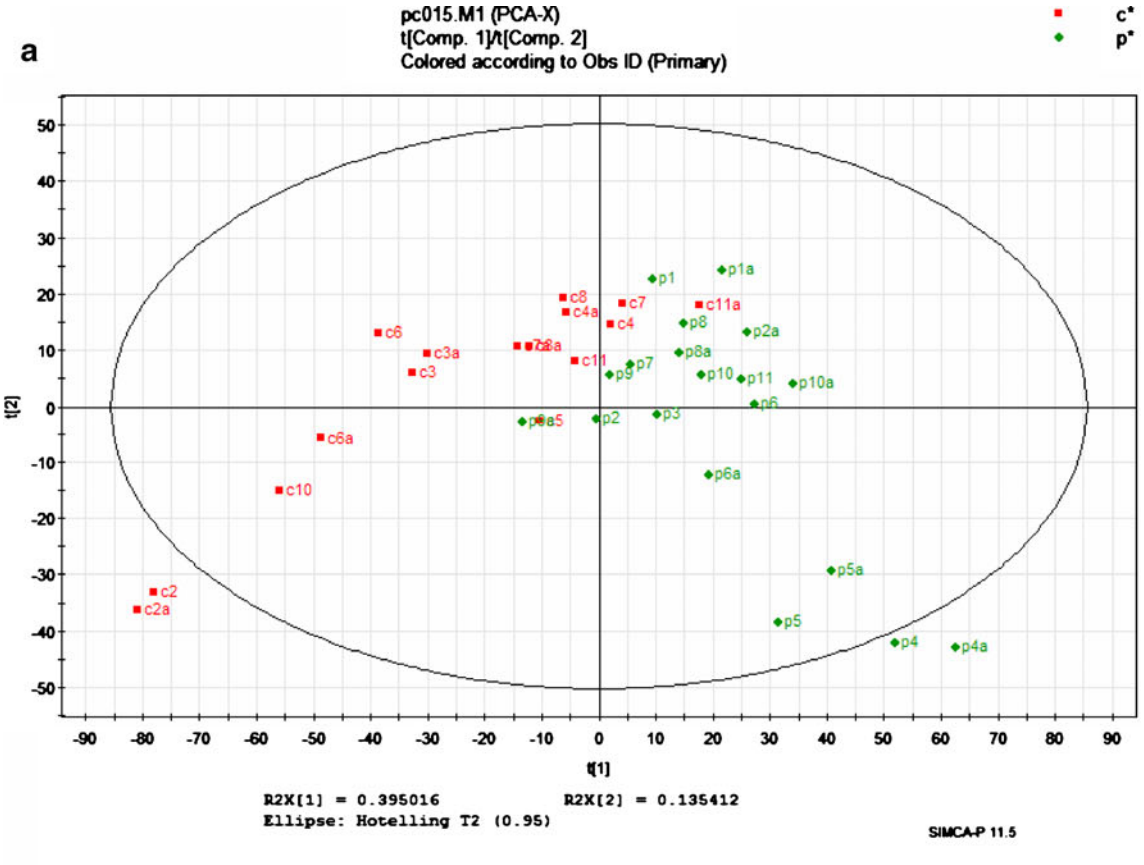
a
pc015.M1 (PCA-X)
t[Comp. 1]/t[Comp. 2]
Colored according to Obs ID (Primary)
c*
p*
t[2]
t[1]
R2X[1] = 0.395016
R2X[2] = 0.135412
Ellipse: Hotelling T2 (0.95)
SIMCA-P 11.5

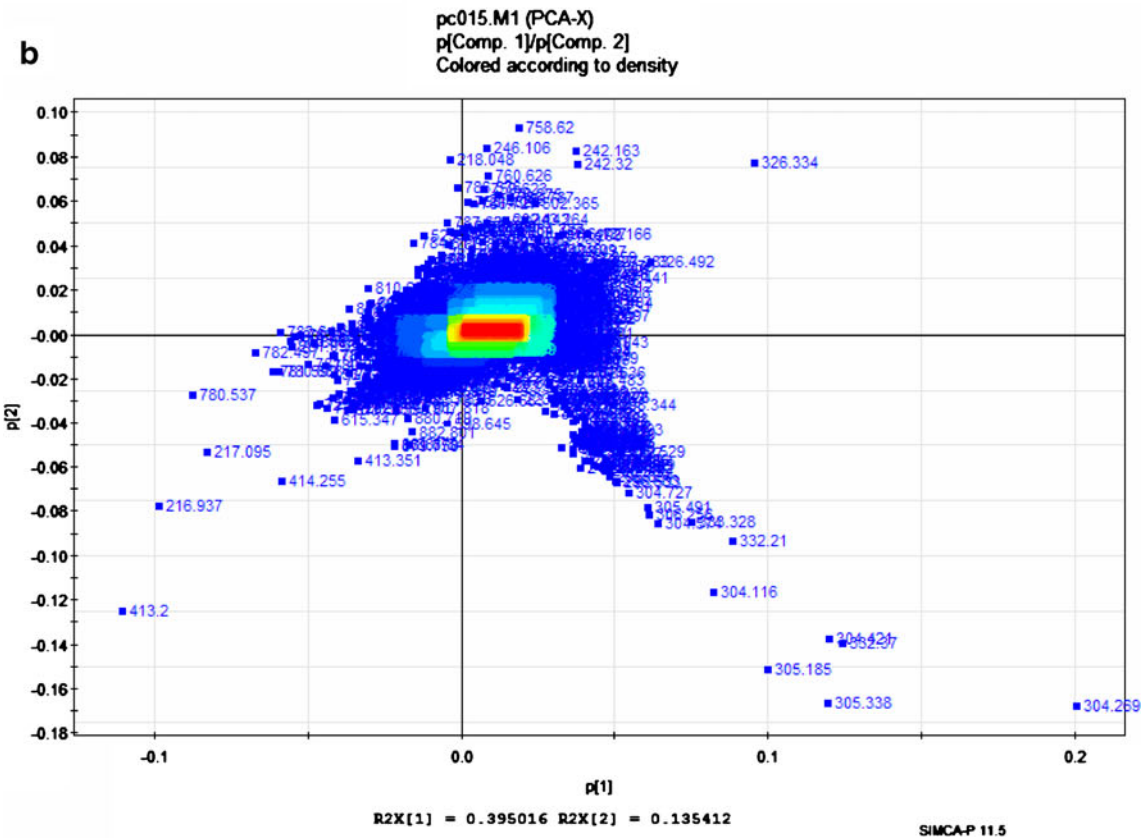
b
pc015.M1 (PCA-X)
p[Comp. 1]/p[Comp. 2]
Colored according to density
p[2]
p[1]
R2X[1] = 0.395016 R2X[2] = 0.135412
SIMCA-P 11.5

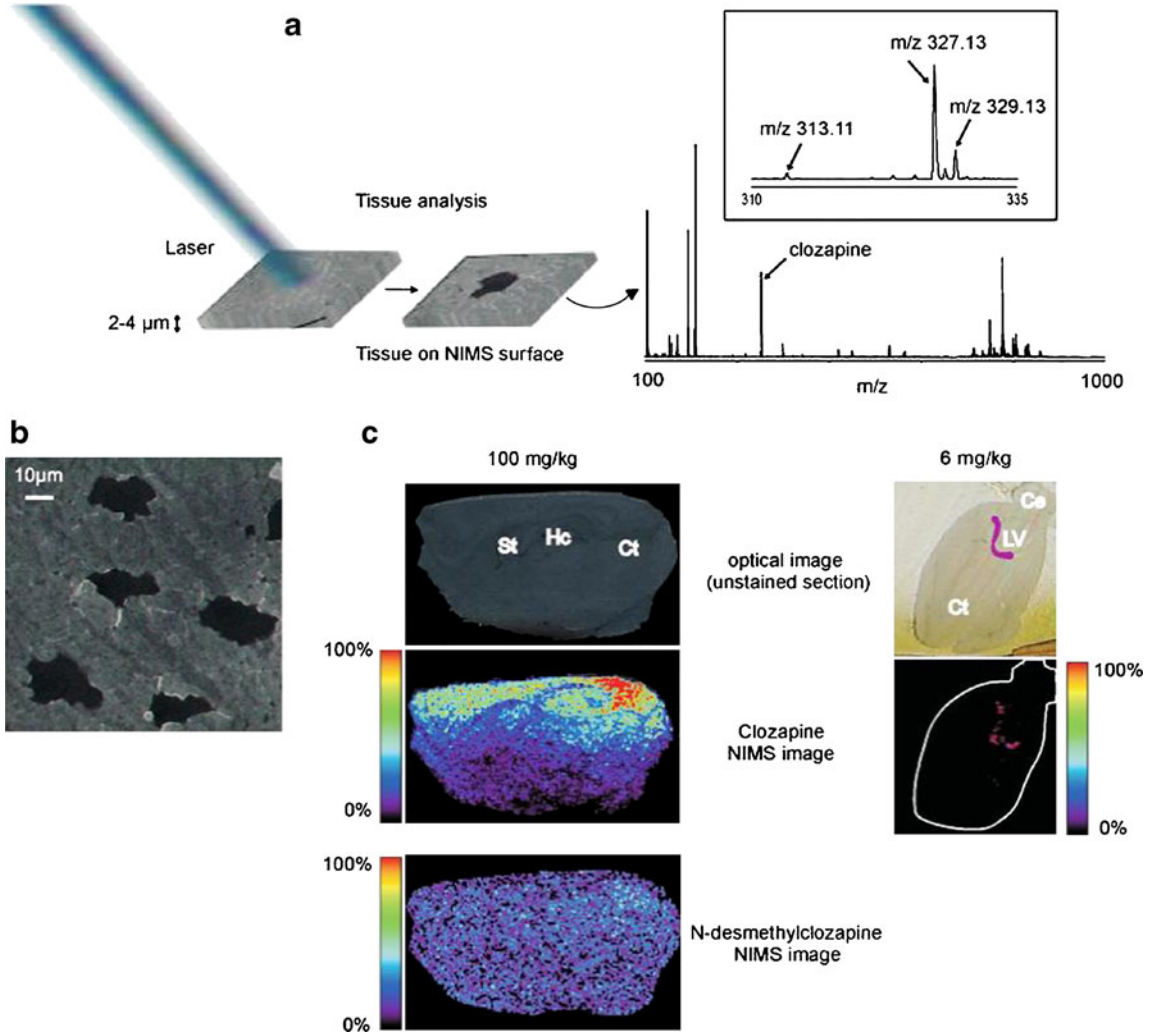

Fig. 16 **a**, **c** The concept of tissue imaging with laser NIMS. **a** The tissue slice (2–4 μm thick sections) is placed directly on the surface and subjected to ~0.1 Jcm^{-2}/pulse laser irradiation, resulting in the desorption/ionisation of endogenous metabolites and xenobiotics. A NIMS mass spectrum shows the detection of clozapine $[M+H]^+$ (*m/z* 327.13) and *N*-desmethylclozapine $[M+H]^+$ (*m/z* 313.11) in the brain tissue. *Inset* shows a magnified region. **b** Nitrogen laser beam irradiation produces 15–20 μm diameter burn marks (*black area*). The optical image shows the sagittal unstained section of a mouse brain after MS acquisition. **c** *Top*: unstained sections of brain slices (sagittal) before NIMS analysis. *Hc*, hippocampus; *St*, striatum; *Ce*, cerebellum; *LV*, lateral ventricle; *Ct*, cortex. *Middle*: NIMS clozapine images (dose: 100 mg/kg rat and 6 mg/kg mouse). *Bottom*: NIMS *N*-desmethylclozapine image (dose: 100 mg/kg). For easy visualization, the *purple mark in the unstained section* (6 mg/kg) indicates clozapine localization by NIMS. In the NIMS image, the edge of the tissue has been also *highlighted in white*. Reproduced with permission from [142]; copyright 2009, *Analytical Chemistry*

olites secreted) of yeast (*Saccharomyces cerevisiae*) using DIOS-MS was feasible [134] (Fig. 13). Previously, similar studies have been demonstrated by the same group using direct infusion mass spectrometry (DIMS) with electrospray ionisation [135]. A large number of metabolic profiles from wild types and mutants were collected, and the data set was analysed by multivariate data analysis to determine potential biomarkers. Principal component analysis (PCA) was performed using a nonlinear iterative partial least squares (NIPALS) algorithm, and a selected number of PCs (those which contributed to more than 95% of the explained variance) were chosen for discriminant function analysis (DFA). Clustering in the PC-DFA space was then studied. This approach identified biomarker candidates that distinguished the wild types from the mutants. The results could aid the calculation of gene expression under environmental influences or enable speculation on the possible metabolic pathways [134]. Still, because DIOS-MS lacked quantitative ability without the aid of an isotopic internal standard, DIMS was also used at the same time to assist data interpretation. The profiling of endogenous metabolites of yeast was also reported by Amantonico et al. using NIMS in negative ion mode [136]. Various phosphorylated nucleotides were detected and identified by making reference to standard compounds. However, accurate mass/lock mass or PSD was not performed. The reason that the negative mode was

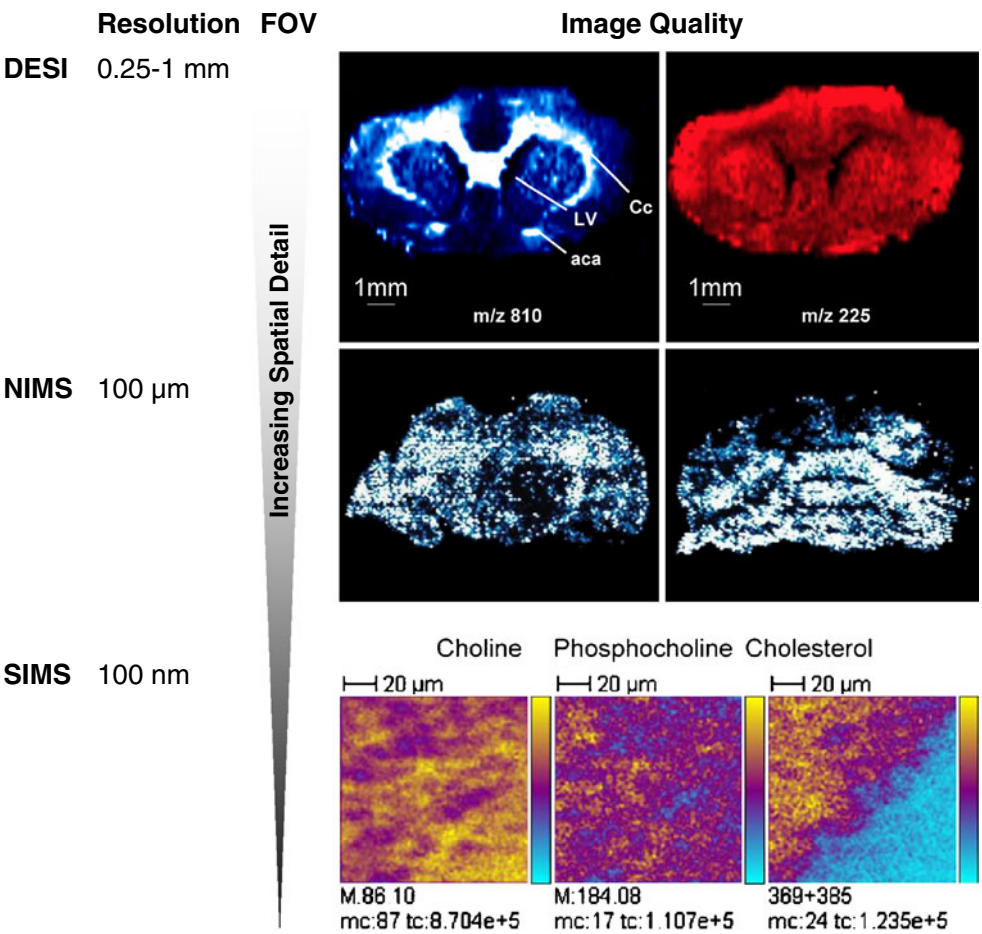

Fig. 17 Image quality comparison for DESI, NIMS and SIMS IMS. Images are of rodent brain tissue and are extracted from [143–145]. Images are reproduced with the permission of the *International Journal of Mass Spectrometry* (copyright 2007), and *Analytical Chemistry* (copyright 2010)

preferred over the positive mode was that only adenosine nucleotides could be detected in the positive mode [137]. It was also noted that the selection of the initiator was critical to the successful analysis of the nucleotides (Fig. 14).

Clinical diagnosis

A metabolic profiling approach can also be effectively applied to clinical applications [138]. In a preliminary study carried out by the authors, the plasma extracts obtained from patients who suffered from polycystic ovarian syndrome (POS) were studied by DIOS-MS. The DIOS metabolic profiles generated were compared with those of healthy subjects. Multivariate statistical analysis was then applied to evaluate the data generated (Fig. 15). The procedures used for data conversion, filtering, peak alignment, normalisation and statistical analysis were the same as those described in [138]. It can be seen from the PCA loading plot that the patient and the control groups are separated with an overlap of <10%. The information obtained can be used to estimate disease progression and the effect of medical treatment. The control c2 was identified as an outlier and was diagnosed with a different medical condition. The ions corresponding to the differences between the patient and the control groups can easily be identified in the PCA score plot, and (as discussed above) can provide information to determine biomarker candidates.

Imaging mass spectrometry (IMS)

Normally, biological compounds are extracted into a solution and deposited onto the substrate prior to mass spectrometric study. Given that SALDI is a surface mass spectrometric technique similar to MALDI and secondary ion mass spectrometry (SIMS), small-molecule IMS is possible. He et al. were the first to demonstrate that SALDI-IMS of biological tissue was achievable [139]. Two-dimensional ion images of mouse liver tissue and human cervical cancer cells were obtained. The density or the thickness of the biological tissue was important, since laser radiation must penetrate through the tissue sample and be absorbed by the PSi layer underneath. To overcome this limitation, organic matrix was sublimated onto the tissue section in subsequent studies [140, 141]. This approach was termed matrix-enhanced surface-assisted laser desorption/ionisation mass spectrometry (ME-SALDI-MS) to indicate the hybrid nature of the technique and the enhancement achieved. 2D ion images of mouse heart and brain tissue

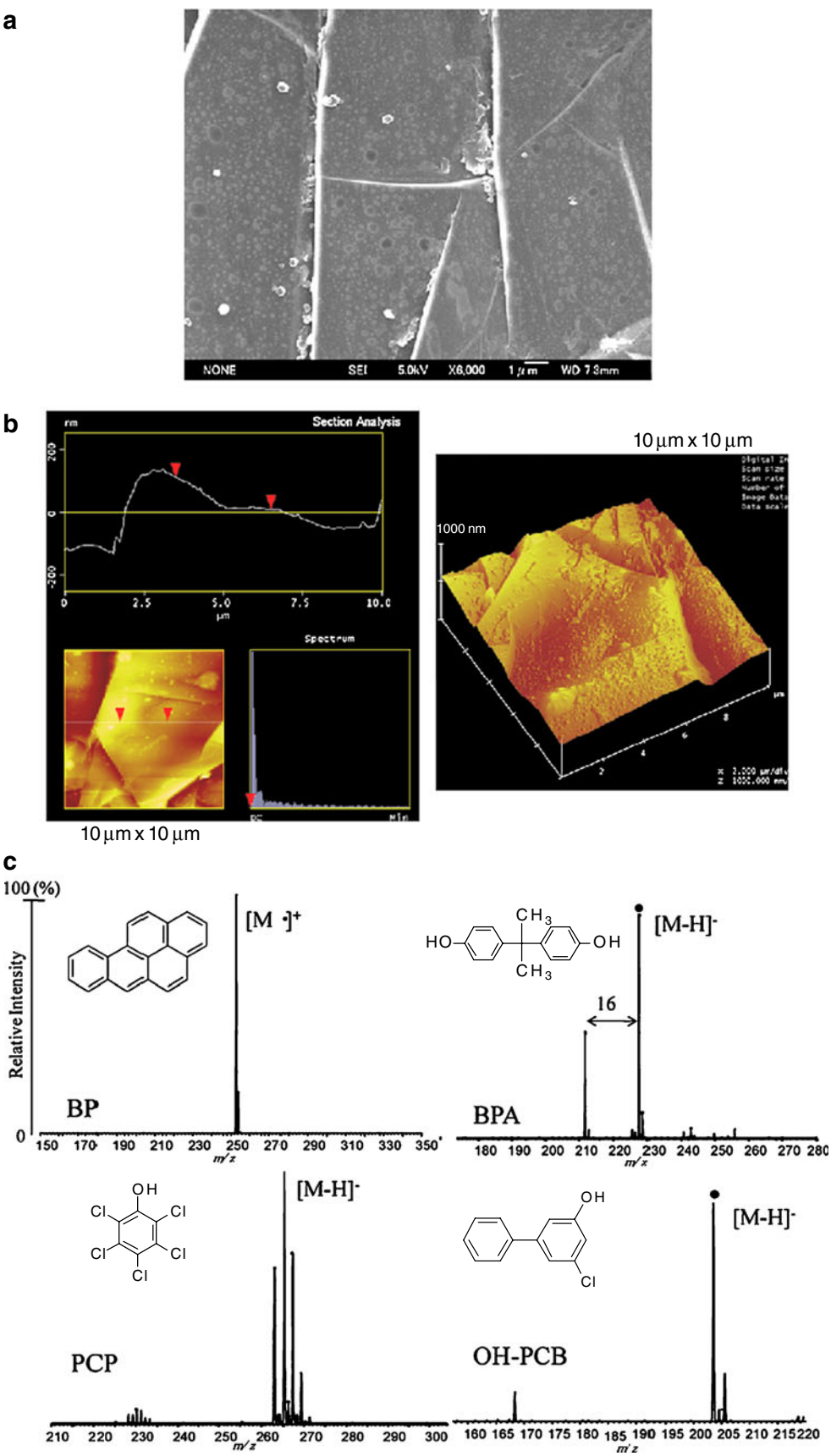

Fig. 18 **a** SEM image and **b** AFM topographic analysis of the highly oriented graphite polymer film. **c** PGS-SALDI mass spectra of benzo[a]pyrene (BP), bisphenol A (BPA), pentachlorophenol (PCP) and 4-hydroxy-2-chlorobiphenyl (OH-PCB). *Insets* show the chemical structures of these species. Reproduced with permission from [146]; copyright 2009, *Rapid Communications in Mass Spectrometry*

were also successfully obtained. Siuzdak et al. also exploited NIMS for IMS. Ion images of the drug molecule distribution in brain tissue (Fig. 16), the cholesterol distribution in brain tissue and the sucrose distribution in a *Gerbera jamesonii* flower stem were demonstrated [142, 143]. SALDI has advantages over MALDI, SIMS and desorption electrospray ionisation (DESI) in small-molecule IMS because of the matrix background interference in MALDI, the extensive fragmentation in SIMS and the relatively low spatial resolution in DESI [144, 145] (Fig. 17). Direct analysis of drug molecules and their metabolites from biofluids was also demonstrated in [142].

Analysis of environmental pollutants

Using pyrolytic highly oriented graphite polymer film (PGS), various environmental pollutants, including perfluorooctanoic sulfonic acid (PFOS), perfluorooctanoic acid (PFOA), benzo[a]pyrene (BP), bisphenol A (BPA), pentachlorophenol (PCP), 4-hydroxy-2-chlorobiphenyl (OH-PCB), 4-chloroaniline (4-CA) and 2,4-dichloroaniline (2,4-CA) were investigated by Kawasaki et al. (Fig. 18) [146]. The investigation of PFOS and PFOA was previously carried out using DIOS-MS in negative ion mode [147], and a detection limit of 1 ppt was achieved for PFOS. This sensitivity could not be achieved by MALDI or LC-ESI-MS, and this highlights a unique ability of DIOS. PFOS in the tap water (water service at Osaka in Japan) was quantified (8.7±2.2 ppt) using sodium dodecyl-d_{25} sulfate (SDS-d_{25}) as an internal standard. Although DIOS showed a high performance in the detection of PFOS, the sensitivity of PFOA was relatively poor. A new method that used oxidised PGS modified with the cationic polymer polyethyleneimine (PEI) was found to be more suitable for the analysis of PFOA. The PFOA content in river water collected from the Kanzaki River in Osaka, Japan was quantified (50±20 ppb) using PFOA-$^{13}C_8$ as an internal standard. All of these results were in agreement with those obtained by LC-MS/MS.

Other environmental pollutants (PFOS, BP, BPA, PCP and OH-PCB) were also detected efficiently by PGS-SALDI as the protonated or deprotonated molecular ion. The authors stressed that these compounds would have been difficult to detect simultaneously by GC-MS or LC-MS. Detailed examination of the PGS-SALDI mass spectra revealed that BP was photoionised and detected as a radical cation in positive ion mode. BPA, PCP and OH-PCB were detected as deprotonated molecules in negative ion mode. Interestingly, the spectrum of BPA shows a peak located *m/z* 16 lower than the $[M–H]^-$ peak of BPA, which (in our view) could be a CH_4 neutral loss fragment peak of BPA. Nevertheless, for reasons unclear to the authors, 4-CA and 2,4-CA were not detected. As mentioned earlier, photoexcitation plays an important role in SALDI. A possible reason (in our view) is that UV radiation excites the electrons of the halo-aromatic system, and the electrons are promoted to the π* state. The interaction of the non-bonding pair of electrons on a substitute with the π electron has the effect of stabilising the π* state, thereby lowering its energy. This induces an opposite effect to oxygen and nitrogen. For oxygen, delocalisation of its lone pairs of electrons with the excited halo-aromatic system favours deprotonation. However, delocalisation of the lone pair of electrons located at the nitrogen of the amine group reduces its electron density, which does not favour protonation. The formation of anilinium cation results in loss of a lone pair interacting with the π* state and is energetically unfavourable. Deprotonation of aniline in the gas phase requires a relatively large input of energy. The calculated deprotonation energy of aniline at the amine nitrogen is 1534 ± 8 kJ mol^{-1}. The calculated values are 121, 145 and 151 kJ mol^{-1} higher at C2, C3 and C4 positions, respectively [148]. The relative position of the chorine in the aromatic system also has an effect. For both 4-CA and 2,4-CA, the chlorine atoms are located at the *ortho* and/or *para* positions, and this induces a stronger electron-withdrawing effect than a chlorine located at the *meta* position.

Conclusions

For the past decade, progress in systems biology and pharmaceutical development has required innovation in the analytical sciences. Mass spectrometry, one of the most powerful and sensitive analytical platforms available, is at the forefront of attempts to answer the challenges presented by systems biology and other areas of analytical and bioanalytical chemistry. Many new mass spectrometry technologies and applications have emerged and been reported. Under these circumstances, SALDI-MS has been reinvented. The technique has now developed into a number of varieties that are vastly different from that originally proposed. Thus, standardisation of terminology is needed. The most significant development of the technique has involved the use of nanomaterials, such as CNTs, metallic nanoparticles (mostly silver, platinum and gold) and nanostructured surfaces. The development of DIOS-MS in particular, and subsequently NIMS and NALDI, has attracted the attention of analytical scientists. These methods have since become a benchmark for semiconductor-based SALDI research. SALDI-MS has many advantages, and the potential applications of the technique are extremely wide. In the authors' view, the selected chemical and biomedical applications are of particular interest because these applications make use of the advantages of the technique and are relatively difficult or are less suitable to perform using other mass spectrometry approaches. On the other hand, the

elucidation of the SALDI ionisation mechanism was controversial. Available data were scattered, inconsistent and complicated by the different experimental conditions employed by different researchers. Data interpretation was often subjective, and much was speculated or unsupported. However, some knowledge has accumulated, and this has influenced the direction of SALDI development. SALDI shares many features with other laser mass spectrometry techniques and, as with MALDI, multiple interrelated excitation and ionisation reactions occur simultaneously. The difference is that the functions of the matrix are substituted by an active substrate. It is foreseeable that substrate development and the exploration of novel biomedical, clinical, chemical and environmental applications will continue.

References

1. Sunner J, Dratz E, Chen Y-C (1995) Anal Chem 67:4335–4342
2. Han M, Sunner J (2000) J Am Soc Mass Spectrom 11:644–649
3. Tanaka K, Waki H, Ido Y, Akita S, Yoshida Y, Yoshida T (1988) Rapid Commun Mass Spectrom 2:151–153
4. Zhang Q, Zou H, Guo Z, Zhang Q, Chen X, Ni J (2001) Rapid Commun Mass Spectrom 15:217–223
5. Hoang TT, Chen Y, May SW, Browner RF (2004) Anal Chem 76:2062–2070
6. Peterson DS (2007) Mass Spectrom Rev 26:19–34
7. Pan C, Xu S, Zhou H, Fu Y, Ye M, Zou H (2007) Anal Bioanal Chem 387:193–204
8. Cohen L, Go EP, Siuzdak G (2007) Small-molecule desorption/ionization mass analysis. In: Hillenkamp F, Peter-Katalinić J (eds) MALDI MS: a practical guide to instrumentation, methods and applications, 1st edn. Wiley-VCH, Weinheim
9. Law KP (2010) Int J Mass Spectrom 290:47–59
10. Law KP (2010) Int J Mass Spectrom 290:72–84
11. Kang M-J, Pyun J-C, Lee J-C, Choi Y-J, Park J-H, Park J-G, Lee J-G, Choi H-J (2005) Rapid Commun Mass Spectrom 19:3166–3170
12. Daniels RH, Dikler S, Li E, Stacey C (2008) J Assn Lab Automation 13:314–321
13. IUPAC (2004) Project: Standard definitions of terms relating to mass spectrometry. http://www.iupac.org/web/ins/2003-056-2-500. Accessed 23 April 2010
14. Guo Z, Ganawi A, Liu Q, He L (2006) Anal Bioanal Chem 384:584–592
15. Iijima S (1991) Nature 354:56–58
16. Mizuno K, Ishii J, Kishida H, Hayamizu Y, Yasuda S, Futaba DN, Yumura M, Hata K (2009) Proc Natl Acad Sci USA 106:6044–6047
17. Shin SJ, Choi D-W, Kwak H-S, Lim GI, Choi YS (2006) Bull Korean Chem Soc 27:581–583
18. Dattelbaum AM, Iyer S (2006) Expert Rev Proteomics 3:153–161
19. Najam-ul-Haq M, Rainer M, Szabó Z, Vallant R, Huck CW, Bonn GK (2007) J Biochem Biophys Methods 70:319–328
20. Xu S, Li Y, Zou H, Qiu J, Guo Z, Guo B (2003) Anal Chem 75:6191–6195
21. Pan C, Xu S, Zou H, Guo Z, Zhang Y, Guo B (2004) J Am Soc Mass Spectrom 16:263–270
22. S-f Ren L, Zhang Z-h Cheng, Guo Y-l (2005) J Am Soc Mass Spectrom 16:333–339
23. Ren S-f, Guo Y-l (2005) Rapid Commun Mass Spectrom 19:255–260
24. Pan C, Xu S, Hu L, Su X, Ou J, Zou H, Guo Z, Zhang Y, Guo B (2005) J Am Soc Mass Spectrom 16:883–892
25. Chen W-Y, Wang L-S, Chiu H-T, Chen Y-C, Lee C-Y (2004) J Am Soc Mass Spectrom 15:1629–1635
26. Tang H-W, Ng K-M, Lu W, Che C-M (2009) Anal Chem 81:4720–4729
27. Alimpiev S, Nikiforov S, Karavanskii V, Minton T, Sunner J (2001) J Chem Phys 115:1891–1901
28. Shariatgorji M, Amini N, Thorsen G, Crescenzi C, Ilag LL (2008) Anal Chem 80:5515–5523
29. Amini N, Shariatgorji M, Thorsén G (2009) J Am Soc Mass Spectrom 20:1207–1213
30. Amini N, Shariatgorji M, Crescenzi C, Thorsén G (2010) Anal Chem 82:290–296
31. Ugarov MV, Egan T, Khabashesku DV, Schultz JA, Peng H, Khabashesku VN, Furutani H, Prather KS, Wang HWJ, Jackson SN, Woods AS (2004) Anal Chem 76:6734–6742
32. Wei J, Buriak J, Siuzdak G (1999) Nature 399:243–246
33. Lewis W, Shen Z, Finn MG, Siuzdak G (2003) Int J Mass Spectrom 226:107–116
34. Nordstrom A, He L, Siuzdak G (2007) Desorption/ionization on silicon (DIOS). In: Gross ML, Caprioli RM (eds) The encyclopedia of mass spectrometry volume 6: molecular ionization methods, 1st edn. Elsevier, Amsterdam
35. Shen Z, Thomas JJ, Averbuj C, Broo KM, Engelhard M, Crowell JE, Finn MG, Siuzdak G (2001) Anal Chem 73:612–619
36. Stewart MP, Buriak JM (2000) Adv Mater 12:859–869
37. Schmeltzer JM, Buriak JM (2004) Recent developments in the chemistry and chemical applications of porous silicon. In: Rao CNR, Müller A, Cheetham AK (eds) The chemistry of nanomaterials: synthesis, properties and applications, vol 2. Wiley-VCH, Weinheim
38. Canham LT (1990) Appl Phys Lett 57:1046–1048
39. Northen TR, Yanes O, Northen MT, Marrinucci D, Uritboonthai W, Apon J, Golledge SL, Nordstrom A, Siuzdak G (2007) Nature 449:1033–1036
40. Kalkan AK, Bae S, Li H, Hayes DJ, Fonash SJ (2000) J Appl Phys 88:555–561
41. Kalkan AK, Henry MR, Li H, Cuiffi JD, Hayes DJ, Palmer C, Fonash SJ (2005) Nanotechnology 16:1383–1391
42. Seino T, Sato H, Yamamoto A, Nemoto A, Torimura M, Tao H (2007) Anal Chem 79:4827–4832
43. Sato H, Nemoto A, Yamamoto A, Tao H (2009) Rapid Commun Mass Spectrom 23:603–610
44. Finkel NH, Prevo BG, Velev OD, He L (2005) Anal Chem 77:1088–1095
45. Xiao Y, Retterer ST, Thomas DK, Tao J-Y, He L (2009) J Phys Chem C 113:3076–3083
46. Go EP, Apon JV, Luo G, Saghatelian A, Daniels RH, Sahi V, Dubrow R, Cravatt BF, Vertes A, Siuzdak G (2005) Anal Chem 77:1641–1646
47. Luo G, Chen Y, Daniels H, Dubrow R, Vertes A (2006) J Phys Chem B 110:13381–13386
48. Coffinier Y, Janel S, Addad A, Blossey R, Gengembre L, Payen E, Boukherroub R (2007) Langmuir 23:1608–1611
49. Hayes DJ (2004) Micrototal analysis system for enzymatic drug metabolism and analysis (Ph.D. thesis). Department of Engineering Science and Mechanics, Pennsylvania State University, University Park
50. Okuno S, Arakawa R, Okamoto K, Matsui Y, Seki S, Kozawa T, Tagawa S, Wada Y (2005) Anal Chem 77:5364–5369
51. Shin JH, Song JY, Park HM (2009) Mater Lett 63:145–147
52. Shin WJ, Shin JH, Song JY, Han SY (2010) J Am Soc Mass Spectrom 21:989–92
53. Chen Y, Vertes A (2006) Anal Chem 78:5835–5844
54. Chen Y, Luo G, Diao J, Chornoguz O, Reeves M, Vertes A (2007) J Phys Conf Ser 59:548–554
55. Sainiemi L, Keskinen H, Aromaa M, Luosujärvi L, Grigoras K, Kotiaho T, Mäkelä JM, Franssila S (2007) Nanotechnology 18:505303–505310

56. Jokinen V, Aura S, Luosujärvi L, Sainiemi L, Kotiaho T, Franssila S, Baumann M (2009) J Am Soc Mass Spectrom 20:1723–1730
57. Wen X, Dagan S, Wysocki VH (2007) Anal Chem 79:434–444
58. Dagan S, Hua Y, Boday DJ, Somogyi A, Wysocki RJ, Wysocki VH (2009) Int J Mass Spectrom 283:200–205
59. Watanabe T, Kawasaki H, Yonezawa T, Arakawa R (2008) J Mass Spectrom 43:1063–1071
60. Dattelbaum AM, Hicks RK, Shelley J, Koppisch AT, Iyer S (2008) Micropor Mesopor Mat 114:193–200
61. Shariatgorji M, Amini N, Ilag L (2009) J Nanopart Res 11:1509–1512
62. Li J, Lu C, Hu XK, Yang X, Loboda AV, Lipson RH (2009) Int J Mass Spectrom 285:137–142
63. Gl Piret, Drobecq H, Coffinier Y, Melnyk O, Boukherroub R (2010) Langmuir 26:1354–1361
64. Shenar N, Cantel S, Martinez J, Enjalbal C (2009) Rapid Commun Mass Spectrom 23:2371–2379
65. Guénin E, Lecouvey M, Hardouin J (2009) Rapid Commun Mass Spectrom 23:1395–1400
66. Li X, Bohn PW (2000) Appl Phys Lett 77:2572–2574
67. Kruse RA, Li X, Bohn PW, Sweedler JV (2001) Anal Chem 73:3639–3645
68. Li Q, Ricardo A, Benner SA, Winefordner JD, Powell DH (2005) Anal Chem 77:4503–4508
69. Tsao C-W, Kumar P, Liu J, DeVoe DL (2008) Anal Chem 80:2973–2981
70. Skipp P, Farooqui M, Pickard K, Li Y, Evans AGR, O'Connor CD (2004) Expanding the information window to increase proteomic sensitivity and selectivity. In: Valdes JJ, Sekowski JW (eds) Proceedings of NATO Advanced Workshop on Proteomics and Toxicogenomics. IOS Press, Amsterdam
71. Li Q (2005) Exploring desorption/ionization on porous silicon mass spectrometry and its applications (Ph.D. thesis). Department of Chemistry, University of Florida, Gainesville
72. Tsao C-W (2008) Interfacing microfluidic bioanalysis with high sensitivity mass spectrometry (Ph.D. dissertation). Department of Mechanical Engineering, University of Maryland, College Park
73. Piret G, Coffinier Y, Roux C, Melnyk O, Boukherroub R (2008) Langmuir 24:1670–1672
74. Alimpiev S, Grechnikov A, Sunner J, Karavanskii V, Simanovsky Y, Zhabin S, Nikiforov S (2008) J Chem Phys 128:014711–014719
75. Hanley L, Kornienko O, Ada ET, Fuoco E, Trevor JL (1999) J Mass Spectrom 34:705–723
76. Zhu X (1994) Annu Rev Phys Chem 45:113–144
77. Knochenmuss R (2002) J Mass Spectrom 37:867–877
78. Knochenmuss R (2006) Analyst 131:966–986
79. Kolasinski K (2002) Surface science: foundations of catalysis and nanoscience. Wiley, Chichester
80. Stewart MP, Buriak JM (2001) J Am Chem Soc 123:7821–7830
81. Budimir N, Fournier F, Blais J-C, Wind F, Tabet J-C (2003) Study of fatty acids and sulfonic acids by desorption/ionization on silicon mass spectrometry. In: 51st Annu Conf ASMS, Montreal, Canada, 8–12 June 2003
82. Okuno S, Arakawa R, Wada Y (2004) J Mass Spectrom Soc Jpn 52:13–20
83. Okuno S, Nakano M, G-e Matsubayashi, Arakawa R, Wada Y (2004) Rapid Commun Mass Spectrom 18:2811–2817
84. Budimir N, Blais J-C, Fournier F, Tabet J-C (2007) J Mass Spectrom 42:42–48
85. Umezu I, Kohno K, Aoki K, Kohama Y, Sugimura A, Inada M (2002) Vacuum 66:453–456
86. Nayak R, Knapp DR (2007) Anal Chem 79:4950–4956
87. Xu D, Guo G, Gui L, Tang Y, Zhang B, Qin G (1998) Electrochem Solid-State Lett 1:227–229
88. Xu D, Guo G, Gui L, Tang Y, Zhang BR, Qin GG (1999) J Phys Chem B 103:5468–5471
89. Xu D, Guo G, Gui L, Tang Y, Qin GG (2000) Pure Appl Chem 72:237–243
90. Cullis AG, Canham LT, Calcott PDJ (1997) J Appl Phys 82:909–965
91. Palaria A, Klimeck G, Strachan A (2008) Electronic structure and transport in silicon nano-structures with non-ideal bonding environments. TECHCON, Austin
92. Maus M, Ganteför G, Eberhardt W (2000) Appl Phys A 70:535–539
93. Kottmann JP, Martin OJF, Smith DR, Schultz S (2000) Opt Express 6:213–219
94. Northen TR, Woo HK, Northen MT, Nordström A, Uritboonthail W, Turner KL, Siuzdak G (2007) J Am Soc Mass Spectrom 18:1945–1949
95. Wada Y, Yanagishita T, Masuda H (2007) Anal Chem 79:9122–9127
96. Luo G, Chen Y, Siuzdak G, Vertes A (2005) J Phys Chem B 109:24450
97. Nordstrom A, Apon JV, Uritboonthai W, Go EP, Siuzdak G (2006) Anal Chem 78:272–278
98. Vertes A (2007) Soft laser desorption ionization—MALDI, DIOS and nanostructures. In: Phipps CR (ed) Laser ablation and its applications. Springer, New York
99. Gloria R, Lichtenberg J, Hierlemann A, Poulikakos D (2005) Micro platform for investigation of explosive vaporization in micro enclosures. In: 9th Int Conf on Miniaturized Systems for Chemistry and Life Sciences (μTAS), Boston, MA, USA, 9–13 Oct 2005
100. Huwe A, Kremer F, Behrens P, Schwieger W (1999) Phys Rev Lett 82:2338–2341
101. Bellissent-Funel M-C, Lal J, Bosio L (1993) J Chem Phys 98:4246–4252
102. Bellissent-Funel M-C, Chen SH, Zanotti J-M (1995) Phys Rev E 51:4558–4569
103. Guégan R, Morineau D, Loverdo C, Béziel W (2006) Phys Rev E 73:011707
104. Chen Y, Chen H, Aleksandrov A, Orlando TM (2008) J Phys Chem C 112:6953–6960
105. King AK, Bellm SM, Hammond CJ, Reid KL, Towrie M, Matousek P (2005) Mol Phys 103:1821–1827
106. Budimir N, Lesage D, Naban-Maillet J, Fournier F, Blais J-C, Wind F, Vékey K, Tabet J-C (2004) Internal energy of ions produced by desorption/ionisation on porous silicon (DIOS). 52nd Annu Conf ASMS, Nashville, TN, USA, 24–27 May 2004
107. Rosenstock HM, Wallenstein MB, Wahrhaftig AL, Eyring H (1952) Proc Natl Acad Sci USA 38:667–678
108. Go EP, Uritboonthai W, Apon JV, Trauger SA, Nordstrom A, O'Maille G, Brittain SM, Peters EC, Siuzdak G (2007) J Proteome Res 6:1492–1499
109. Trauger SA, Go EP, Shen Z, Apon JV, Compton BJ, Bouvier ESP, Finn MG, Siuzdak G (2004) Anal Chem 76:4484–4489
110. Thomas JJ, Blackledge RD, Siuzdak G (2001) Anal Chim Acta 442:183–190
111. Shen ZX, Thomas JJ, Siuzdak G, Blackledge RD (2004) J Forensic Sci 49:1028–1035
112. Pihlainen K, Grigoras K, Franssila S, Ketola R, Kotiaho T, Kostiainen R (2005) J Mass Spectrom 40:539–545
113. Kraj A, Świst M, Strugala A, Parczewski A, Silberringa J (2006) Eur J Mass Spectrom 12:253–259
114. Kraj A, Jarzebinska J, Gorecka-Drzazga A, Dziuban J, Silberring J (2006) Rapid Commun Mass Spectrom 20:1969–1972
115. Bergquist J, Silberring J (1998) Rapid Commun Mass Spectrom 12:683–688
116. Okuno S, Wada Y (2005) J Mass Spectrom 40:1000–1004
117. Finkel NH (2005) Surface-assisted laser desorption/ionization-mass spectrometry (SALDI-MS) of controlled nanofeatures and the associated thermal properties (MSci thesis). Department of Chemistry, North Carolina State University, Raleigh
118. Laiko VV, Taranenko NI, Berkout VD, Musselman BD, Doroshenko VM (2002) Rapid Commun Mass Spectrom 16:1737–1742

119. Thomas JJ, Shen Z, Crowell JE, Finn MG, Siuzdak G (2001) Proc Natl Acad Sci USA 98:4932–4937
120. Go EP, Prenni JE, Wei J, Jones A, Hall SC, Witkowska HE, Shen Z, Siuzdak G (2003) Anal Chem 75:2504–2506
121. Kinumi T, Shimomae Y, Arakawa R, Tatsu Y, Shigeri Y, Yumoto N, Niki E (2006) J Mass Spectrom 41:103–112
122. Go EP, Wikoff WR, Shen Z, O'Maille G, Morita H, Conrads TP, Nordstrom A, Trauger SA, Uritboonthai W, Lucas DA, Chan KC, Veenstra TD, Lewicki H, Oldstone MB, Schneemann A, Siuzdak G (2006) J Proteome Res 5:2405–2416
123. Liesener A, Karst U (2005) Anal Bioanal Chem 382:1451–1464
124. Shen Z, Go EP, Gamez A, Apon JV, Fokin V, Greig M, Ventura M, Crowell JE, Blixt O, Paulson JC, Stevens R, Finn MG, Siuzdak G (2004) ChemBioChem 5:921–927
125. Wall DB, Finch JW, Cohen SA (2004) Rapid Commun Mass Spectrom 18:1482–1486
126. Steenwyk RC, Hutzler JM, Sams J, Shen Z, Siuzdak G (2006) Rapid Commun Mass Spectrom 20:3717–3722
127. Northen TR, Lee J-C, Hoang L, Raymond J, Hwang D-R, Yannone SM, Wong C-H, Siuzdak G (2008) Proc Natl Acad Sci USA 105:3678–3683
128. Nichols KP, Azoz S, Gardeniers HJGE (2008) Anal Chem 80:8314–8319
129. Zou H, Zhang Q, Guo Z, Guo B, Zhang Q, Chen X (2002) Angew Chem Int Ed 41:646–648
130. Hu L, Xu S, Pan C, Zou H, Jiang G (2007) Rapid Commun Mass Spectrom 21:1277–1281
131. Xu S, Pan C, Hu L, Zhang Y, Guo Z, Li X, Zou H (2004) Electrophoresis 25:3669–3676
132. Hollis JM, Lovas FJ, Jewell PR (2000) Astrophys J 540:L107–L110
133. Burke DJ, Brown WA (2010) Phys Chem Chem Phys 12:5947–5969
134. Vaidyanathan S, Jones DG, Ellis J, Jenkins TE, Dunn W, Hayes A, Burton N, Oliver S, Kell DB, Goodacre R (2005) Metabolomics 1:1–8
135. Allen J, Davey H, Broadhurst D, Heald J, Rowland J, Oliver S, Kell D (2003) Nat Biotechnol 21:692–696
136. Amantonico A, Flamigni L, Glaus R, Zenobi R (2009) Metabolomics 5:346–353
137. Gómez D, Fernández JA, Astigarraga E, Marcaide A, Azcárate S (2007) Phys State Solidi (c) 4:2185–2189
138. Miura D, Fujimura Y, Tachibana H, Wariishi H (2010) Anal Chem 82:498–504
139. Liu Q, Guo Z, He L (2007) Anal Chem 79:3535–3541
140. Liu Q, Xiao Y, Pagan-Miranda C, Chiu YM, He L (2009) J Am Soc Mass Spectrom 20:80–88
141. Liu Q, He L (2009) J Am Soc Mass Spectrom 20:2229–2237
142. Yanes O, Woo H-K, Northen TR, Oppenheimer SR, Shriver L, Apon J, Estrada MN, Potchoiba MJ, Steenwyk R, Manchester M, Siuzdak G (2009) Anal Chem 81:2969–2975
143. Patti GJ, Woo H-K, Yanes O, Shriver L, Thomas D, Uritboonthai W, Apon JV, Steenwyk R, Manchester M, Siuzdak G (2010) Anal Chem 82:121–128
144. Ifa DR, Wiseman JM, Song Q, Cooks RG (2007) Int J Mass Spectrom 259:8–15
145. Debois D, Brunelle A, Laprévote O (2007) Int J Mass Spectrom 260:115–120
146. Kawasaki H, Takahashi N, Fujimori H, Okumura K, Watanabe T, Matsumura C, Takemine S, Nakano T, Arakawa R (2009) Rapid Commun Mass Spectrom 23:3323–3332
147. Kawasaki H, Shimomae Y, Watanabe T, Arakawa R (2009) Colloid Surf A 347:220–224
148. Nguyen MT (2007) General and theoretical aspects of anilines. In: Rappoport Z (ed) The Chemistry of Anilines, Part 1 John Wiley & Sons, Chichester, West Sussex, UK